

Satellite Contributions to Surface Heat Budget Estimates: A Study of 4 Ameriflux Sites in Southern California

Tamara Machac

Advisor: Ronald Smith

Yale University

Department of Geology and Geophysics

February 22, 2010

Abstract:

We used data from four Ameriflux tower sites and six Landsat-5 TM satellite images during the summer months of 2007 in Southern California to study the surface heat budget. Our study seeks to determine what information satellites contribute to our ability to estimate surface heat budgets, whether surface heat budgets can provide evidence of an albedo or latent heat feedback, and if we can detect heat budget variations between land cover types. We explore several methods of calculating heat budget terms and examine them over all the sites and dates, by date, and by site. In our findings, we discover that the satellite measures of albedo, NDVI and surface temperature may be better than the ground estimates of these parameters because the satellite's spatial scale is closer to the towers' turbulent flux footprint. We also observe a seasonal signal in the incoming solar radiation and sensible heat flux; however, we find no evidence of an albedo or latent heat feedback. Vegetation cover density was also found to have a significant impact on the albedo, net radiation, sensible heat flux and ground storage flux.

Table of Contents

1	Introduction	3
1.1	Motivation.....	3
1.2	Background	4
2	Methodology	9
2.1	Site Information	9
2.2	Data Sources.....	11
2.2.1	Ground Data	11
2.2.2	Satellite Data	14
2.3.1	Incoming Solar Radiation	18
2.3.2	Albedo	18
2.3.3	Absorbed Solar Radiation	19
2.3.4	Long-Wave Fluxes	19
2.3.5	Net Radiation.....	19
2.3.6	Turbulent Fluxes	20
2.3.7	Imbalance	20
3	Results	25
3.1	All Sites and All Dates.....	25
3.2	Trends by Date	31
3.3	Trends by Site.....	34
4	Implications for Surface Feedbacks	39
5	Satellite Contributions to Surface Heat Budgets	41
6	Conclusions	42
	References	43
	Appendix A: List of Acronyms, Variables and Symbols.....	48
	Appendix B: Landsat-5 TM Pre-processing (Chander and Markham, 2003).....	50
	Appendix C: Ameriflux Site Land-Cover Classifications and Vegetation Types.....	52

1 Introduction

1.1 Motivation

Arid and semi-arid regions cover approximately 40% of the Earth's land surface and are home to approximately 20% of the world's population. These areas have been identified as being particularly sensitive to climate change (Dahm *et al.*, 2002; Malek and Bingham, 1997). This vulnerability stems from natural water scarcity and growing human demand for water in these regions. Local changes in climate can dramatically affect the availability of water (Bates *et al.*, 2008; Christensen *et al.*, 2007; Dahm *et al.*, 2002; Watson *et al.*, 1997; Xu and Haginoya, 2001). The expansion of the African Sahel and Chinese Gobi Desert are possible examples of desertification due to overgrazing and agriculture. An improved understanding of the mechanisms of climate change in these areas is an important goal of climate research.

General circulation models (GCMs) have shown that energy and moisture fluxes between the surface and atmosphere play a significant role in both the short-term (i.e. hours) and long-term (i.e. weeks to months) weather systems that influence regional climate (Christensen *et al.*, 2007). There are two main issues that limit the utility of GCMs for studying regional climate change: lack of accurate surface heat budgets and poorly parameterized surface feedbacks. Few regions have an accurate record of ground data (i.e. surface and atmospheric temperature, incoming and reflected solar radiation, and turbulent heat flux estimates), which are required to calculate a heat budget (Dahm *et al.*, 2002). In areas with little ground data, satellite images provide a practical way to obtain the missing information. Remote sensing measurements of albedo and surface temperature, along with detailed terrain and landscape cover information can improve estimates of the surface heat budget necessary for climate model forecasting (Mahfouf, 1991; Rabin *et al.*, 1990; Zaitchik *et al.*, 2006).

The second problem stems from the limited spatial resolution and ensemble size generally used in climate models (Bates *et al.*, 2008; Christensen *et al.*, 2007; Watson *et al.*, 1997). GCMs which include complex land-surface processes have difficulty anticipating effects on the regional level because of poor land-surface parameterization schemes (Dickinson and Henderson-Sellers, 1988; Lyons *et al.*, 1993). In order to improve these models, it is necessary to determine how different landscapes respond to climate change, what feedbacks dominate when the landscape is changed and how changes in land-cover affect a surface's emitted energy, air temperature, and local feedbacks.

1.2 Background

The energy flux components of a region or surface can be determined from the principles of conservation of energy, where the energy inputs equal the energy outputs. In a simplified daytime surface energy budget (Figure 1), the input terms are solar radiation (solar irradiance), incoming long-wave radiation emitted by the atmosphere (atmospheric irradiance) and the heat flux stored in the ground (ground heat flux). The output terms are: the reflected solar irradiance, long-wave radiation emitted by the surface (earth's irradiance), the turbulent sensible heat flux due to convection and conduction, and turbulent latent heat flux from evaporation. The input terms are considered to be positive to indicate heat flux into the surface, while the output terms are considered to be negative to indicate a loss of heat from the surface. It is important to note that the turbulent heat fluxes and ground heat flux can reverse in direction under certain conditions.

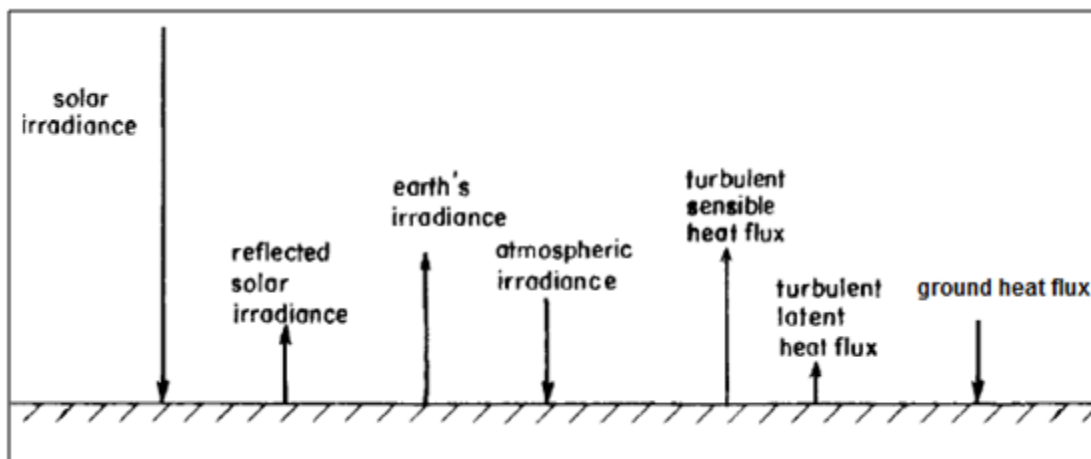


Figure 1: Components of a simplified daytime surface heat budget. The incoming terms are the solar irradiance, atmospheric irradiance, and ground heat flux. The outgoing terms are the reflected solar irradiance, earth's irradiance, the turbulent sensible heat flux, and the turbulent latent heat flux. (Figure modified from Pielke and Avissar, 1990)

Land-use and land-cover are major factors in the heat budgets on regional and local climate scales (Dickinson and Henderson-Sellers, 1988; Lyons et al., 1993; Rabin et al., 1990; Zaitchik et al., 2006). Natural changes in land-cover occur due to the growth or reduction of vegetation cover with seasons as well as climate anomalies, such as seasonal drying or drought events. Human land-use also affects land-cover through agriculture and urban development, for example. When land-cover in an area varies, this affects the albedo, surface roughness, and exchange of water, energy and carbon

dioxide between the surface and the atmosphere. Surfaces with stressed or sparse vegetation due to water scarcity have a higher albedo than surfaces with dense vegetation cover. Increases in surface albedo cause a larger the percentage of the incoming solar radiation to be reflected. If this increase in reflected solar radiation dominates the surface heat budget, this region of high albedo can become a heat sink, creating a regional differential heating pattern with subsiding air suppressing precipitation in an already dry environment. This is an example of a positive climate feedback acting on a regional scale (Charney, 1975; Rabin *et al.*, 1990; Zaitchik *et al.*, 2006).

A number of heat budget studies have been conducted (Brivio *et al.*, 2001; Chehbouni *et al.*, 1997; Ma *et al.*, 2002, 2003, 2004; Malek and Bingham, 1997; Pielke and Avissar, 1990; Tanaka *et al.*, 2001; van den Hurk, 2001; Wang and Liang, 2008; Xu and Haginoya, 2001), each employing a different technique to calculate the surface heat budget. Among these studies, there are two general categories: studies that derive the terms of the heat budget using only meteorological ground data, and studies that make use of a combination of both ground and satellite data to derive the terms of the heat budget. Ground based studies have the advantage of accuracy, however they are limited to the immediate area surrounding the instrument(s). From ground point values alone, it is not possible to estimate the heat budget for a large region with heterogeneous vegetation cover, moisture and terrain. This is where satellite data can help improve heat budget studies, as they allow for a greater area of study with a variety of surface cover. There are three major limitations to satellite heat budget studies: (1) any given satellite image provides information only for the instant the image was taken, (2) atmospheric conditions constrain the number of available images for study, and (3) satellite image pixel values are spatial averages, which can smooth the signal by an amount that depends on the pixel size.

In ground based studies, meteorological stations are used to measure or derive all the terms in the heat budget. Instruments such as pyranometers and radiometers measure incoming and reflected solar radiation as well as incoming and outgoing long-wave radiation. Thermometers can measure air temperature near the surface and at various heights above the ground. Soundings can also provide a temperature profile, however soundings can be even more sparsely distributed across a satellite scene than meteorological stations. Therefore, it is important to note that soundings close to or in the scene of interest are not used as representative of an entire area with variable elevation and ground cover. The amount of heat stored by the surface (ground heat flux) can be calculated from soil temperature probes buried at or beneath the surface. This term is usually estimated as the residual heat needed to balance the budget if the appropriate ground instruments are not available. Ground based studies

commonly calculate the turbulent heat fluxes via the eddy correlation (Tanaka et al., 2001) or Bowen ratio (Malek and Bingham, 1997) methods, which require information about the temporal fluctuations in vertical velocity, temperature and specific humidity across an area.

The work done by Tanaka et al. (2001) and Xu and Haginoya (2001) are examples of studies that employ only meteorological ground data to calculate the terms of the heat budget. Both focus on the evolution of the components of the surface heat budget before, during and after the Asian monsoon in the semi-arid region of Tibet. Tanaka et al. (2001) measure the short-wave and long-wave radiation components using several radiometers and the turbulent sensible and latent heat fluxes via eddy correlation instruments. A large portion of this particular study is dedicated to the comparison of calculated ground heat fluxes using the thermal conductivity and heat diffusion equations with estimates of the ground heat flux as the residual of the surface heat budget. The residual matches the calculated value fairly well during the daytime but overestimates the actual ground heat flux in the late afternoon (by approximately 100 W/m^2) and through the night (by approximately 200 W/m^2). Therefore, the residual cannot be used for the daily averaged energy budget though it is possible to use it for estimates during the daytime. Tanaka et al. (2001) propose that the possible sources for the imbalance are either underestimation of latent heat (sensor instability), or a weak systematic vertical flow (Lee, 1998). Overall, the turbulent flux measurements and the soil heat flux have the largest sources of error.

Xu and Haginoya (2001) use a simple model to estimate seasonal variations in evaporation, soil-water content and soil temperature over regions with bare ground. The input data for the model are solar radiation, humidity, temperature, soil-water content, air temperature, surface temperature, humidity, wind, cloud cover, sunshine duration, and precipitation data from 14 ground stations. This study shows that there is good agreement (less than 5 W/m^2 difference) between the calculated values and the observed values for most of the terms and parameters in the heat budget. Both Tanaka et al. (2001) and Xu and Haginoya (2001) agree that the surface heat budget is dominated by the sensible heat flux in the dry period before the monsoon season.

In studies that use both satellite and ground data, ground measurements, such as atmospheric temperature, sensible heat flux and latent heat flux, are often used in combination with satellite measurements to derive the surface heat budget. Satellites provide band radiance or reflectance data, which are used to estimate the albedo and surface temperature (Brivio et al., 2001, Ma et al., 2002, 2003, 2004). Albedo can be calculated as the simple average or weighted average of the reflective bands

(Liang, 2000; Tasumi, 2008), while the surface temperature can be derived from the satellite's thermal band, using the Planck function (Appendix A). The direct incoming solar radiation can be derived from terrain data, the solar constant, and the solar zenith angle. The diffuse incoming solar radiation can be estimated from model codes such as 6S, which accounts for light scattering and absorption by atmospheric gases and aerosols (Brivio et al., 2001; Vermote, 1996). Other studies similarly use both surface and aerological data in radiative transfer models such as MODTRAN to obtain the total incident short-wave radiation (Ma et al., 2002, 2003, 2004). A commonly used software package known as Solar Analyst Tools in ArcGIS developed by Fu and Rich (2000, 2002) accounts for atmospheric effects, latitude, elevation, steepness, compass direction, daily and seasonal shifts of the solar angle, and shadows cast by topography. This scheme uses three general steps to calculate the solar contribution for each pixel value. First, the software calculates an upward-looking hemispherical viewshed, based on topography. The viewshed is a measure of the amount of visible sky at a given location (e.g. open field vs. deep canyon). Next, this viewshed is overlain on a direct sunmap to estimate direct radiation. The viewshed is also overlain on a diffuse sky map to estimate diffuse radiation. Combining the direct and diffuse radiation gives the total solar radiation contribution for the surface. However, some studies use only ground data to estimate this term; meteorological station point data are extrapolated to the whole image scene (Brivio et al., 2001).

The research conducted by Ma et al. (2002, 2003, 2004, 2006) is an example of a series of studies that examine the use of satellite data in surface heat budget studies. These authors propose a method which includes remote sensing data and models to calculate the surface fluxes for regions of variable land-cover in the Gobi desert. The incoming short- and long-wave radiation are derived from the radiative transfer model, MODTRAN (Berk et al. 1989). The reflected solar radiation is derived using a four-stream radiative transfer assumption, correcting for the atmosphere in the short-wave bands (Verhoef, 1997). The outgoing long-wave radiation is dependent upon the surface emissivity and surface temperature; the surface emissivity is calculated via a vegetation cover model by Valor and Caselles (1996), while the surface temperature is found from the Landsat-5 TM thermal band. Obtaining accurate surface emissivity values is challenging and important because they can vary significantly with ground cover and greatly affect the long-wave radiation emitted by the surface (Zhou et al., 2003). The soil heat flux is found using a relationship defined by Chodury and Monteith (1988), which relies on soil dry bulk density, soil specific heat, surface temperature, soil temperature at a determined depth, and the resistance of heat transport within the soil. The soil heat flux term cannot be directly measured by

the satellite, but some studies show that the soil heat flux can be estimated as a fraction of the net radiation at midday (Daughtry et al., 1990).

In these studies (Ma et al., 2002, 2003, 2004, 2006), the sensible heat flux is calculated using the blending height approach, which assumes that the local advection is small during the time the Landsat image was taken. Atmospheric characteristics are somewhat independent of horizontal position at the “blending height”, which is defined as the height where atmospheric characteristics become roughly independent of the horizontal position. Studies by Lhomme et al. (1994), Bastiaanssen (1995), and Wang et al. (1995) show this method to be successful for calculating the average surface fluxes in a given area. In the blending height approach, the regional sensible heat flux is dependent on blending height as well as the wind speed and air temperature at the blending height. These variables are determined by instruments, such as the radiosonde, tether-sonde and Sodar, and by numerical modeling. The latent heat flux is calculated as the residual of the surface heat budget. The results of these studies show that a good agreement exists (less than 15 % difference) between the field observations and the satellite- and model-derived land surface variables and heat fluxes such as the surface reflectance, surface temperature, net radiation, soil heat flux, and sensible heat flux. Another study conducted by Malek and Bingham (1997) in Nevada similarly indicates agreement between albedo derived from satellite reflective bands and from ground station data. However, Ma et al. (2002, 2003, 2004, 2006) find that calculating the latent heat as the heat budget residual is not a good approach in areas between oasis and desert regions.

Other studies that use a combination of satellite data, ground data, and models, often focus on one or two terms in the heat budget, usually the sensible heat flux and latent heat flux. Several studies (Chehbouni et al., 1997; Cleugh et al., 2007; Pielke and Avissar, 1990; Wang and Liang, 2008) claim that part of the difficulty in calculating sensible and latent heat fluxes via remote sensing is due to differences between radiative surface temperature and aerodynamic surface temperature (differences can exceed 10° C). The aerodynamic surface temperature is associated with the heat exchange efficiency between the surface and the overlying air. It is not possible to measure the aerodynamic surface temperature via satellite, though it may be possible to estimate the aerodynamic surface temperature if given the radiative surface temperature from the satellite and an estimate of the Bowen ratio. Wang and Liang (2008) propose an improvement to an algorithm which seeks to overcome this problem, with promising results. It is important to be able to measure or derive these heat budget terms accurately because the turbulent heat fluxes have a direct effect on the local and regional

weather and climate. Climate change at any scale cannot be reliably assessed unless landscape characteristics and landscape changes are well known (Pielke and Avissar, 1990).

1.3 Objectives

This study has three objectives: (1) to determine what information satellites contribute to our ability to estimate surface heat budgets, (2) to determine whether surface heat budgets provide indications of an albedo or latent heat feedback, and (3) to examine differences in the surface heat budgets between areas of different vegetation cover within a satellite image. Using both satellite and ground data we investigate several methods of calculating the terms of the surface heat budget in the semi-arid region of southern California. By comparing variations in the surface heat budget terms and imbalances between and within six Landsat-5 TM 2007 images, we study the seasonal variations as well as the contribution of land-cover type to the surface heat budget. The heat budget captures a seasonal signal in the incoming solar radiation and sensible heat flux, however, no evidence of an albedo or latent heat feedback was found. Vegetation density has a significant impact on the albedo, net radiation, ground storage flux and sensible heat flux. Much work remains to better understand and estimate regional surface heat budgets. Because ground data is not always available, regional surface heat budget studies require improvements in satellite estimates of all the heat budget terms. While satellites provide fairly accurate information about albedo and surface temperature, more reliable estimates of air temperature and turbulent fluxes from satellite data are needed.

2 Methodology

2.1 Site Information

This study focuses on the region of southern California, April through September of 2007. The area receives most of its rainfall during the winter months and experiences virtually no precipitation throughout the spring, summer and fall. This makes southern CA a good location to test various surface heat budget calculation methods. River discharge data from several USGS river stations in the region (Table 1) show that southern CA is indeed fairly dry throughout the year, with some increase in water flow during the winter, early spring and late fall. Plots from two of these stations are shown in Figure 2.

Station name	Latitude	Longitude
	(deg, min, sec)	(deg, min, sec)
10259200 Deep C NR Palm Desert CA	33 °, 37', 52"	116 °, 23', 29"
10259300 Whitewater R A Indio CA	33 °, 44', 14"	116 °, 14', 07"

Table 1: USGS River Stations (rivers unregulated upstream of stations)

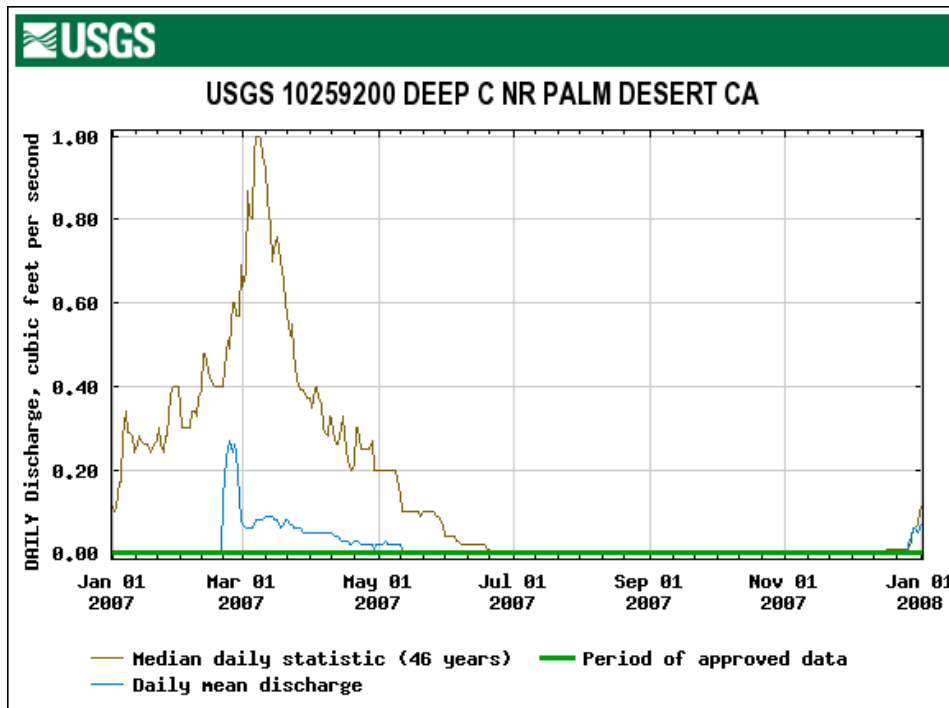


Figure 2a: 2007 Discharge data for USGS station 10259200 Deep C NR Palm Desert CA.

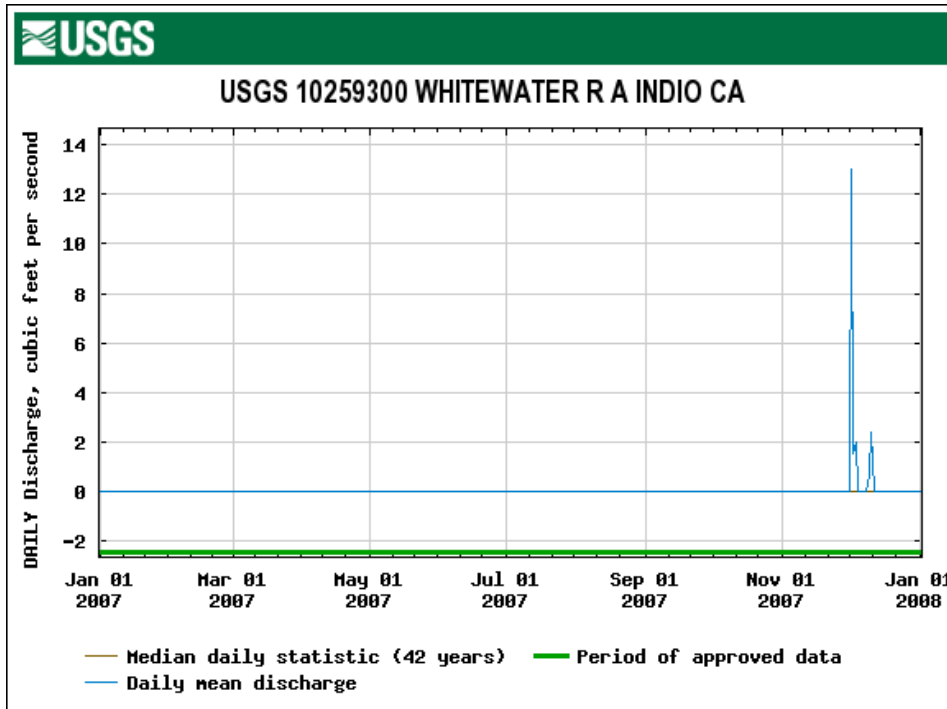


Figure 2b: 2007 Discharge data for USGS station 10259300 Whitewater R A Indio CA.

2.2 Data Sources

2.2.1 Ground Data

The Ameriflux tower network has readily available meteorological data (2006-present) in this region for several different land cover types, including chaparral, desert, grassland, and sage (Table 2 and Figures 3a-d) (e.g. “Ameriflux Network” and Ocheltree and Loescher, 2006). Some measurements were dropped because of obvious internal inconsistencies. For further information about the specific climate and vegetation at each location, see Appendix C.

Site	Latitude (deg, min, sec)	Longitude (deg, min, sec)	Elevation (m)	Terrain Slope (degrees)	Terrain Aspect (degrees)
Chaparral	33 °, 36', 34"	116 °, 27', 2"	1291	4.9	284.9
Desert	33 °, 39', 10"	116 °, 22', 21"	272	2.6	346.0
Grass	33 °, 44', 11"	117 °, 41', 41"	465	5.3	115.0
Sage	33 °, 44', 3"	117 °, 41', 46"	467	6.7	95.4

Table 2: Southern CA Ameriflux tower sites used in this study.

Though the purpose of the Ameriflux network is to provide data to study water vapor and carbon fluxes, the towers also provide data useful for heat budget studies (i.e. incoming and reflected short-wave radiation, net radiation, sensible and latent heat flux, and air temperature). The towers provide data every 30 minutes. We selected data temporally closest to the satellite image acquisition time (approximately 9:30am local solar time). These multiple tower sites situated in areas with different vegetation cover are all located in the same semi-arid region, allowing us to compare differences in the surface heat budget among different land cover types all subjected to the same overall climate.

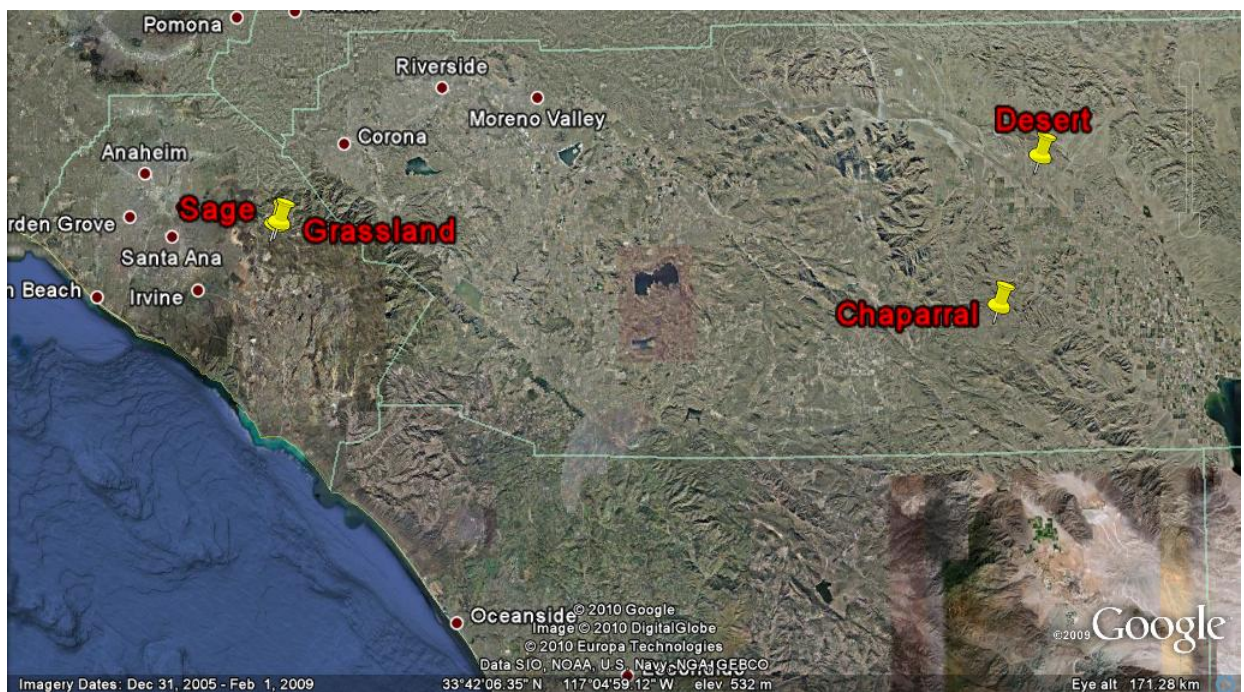


Figure 3a: Southern CA Ameriflux tower sites: Chaparral, Desert, Grassland and Sage (located using Google Earth). The Grassland and Sage sites are located relatively close to each other, making it difficult to distinguish between them at this magnification.

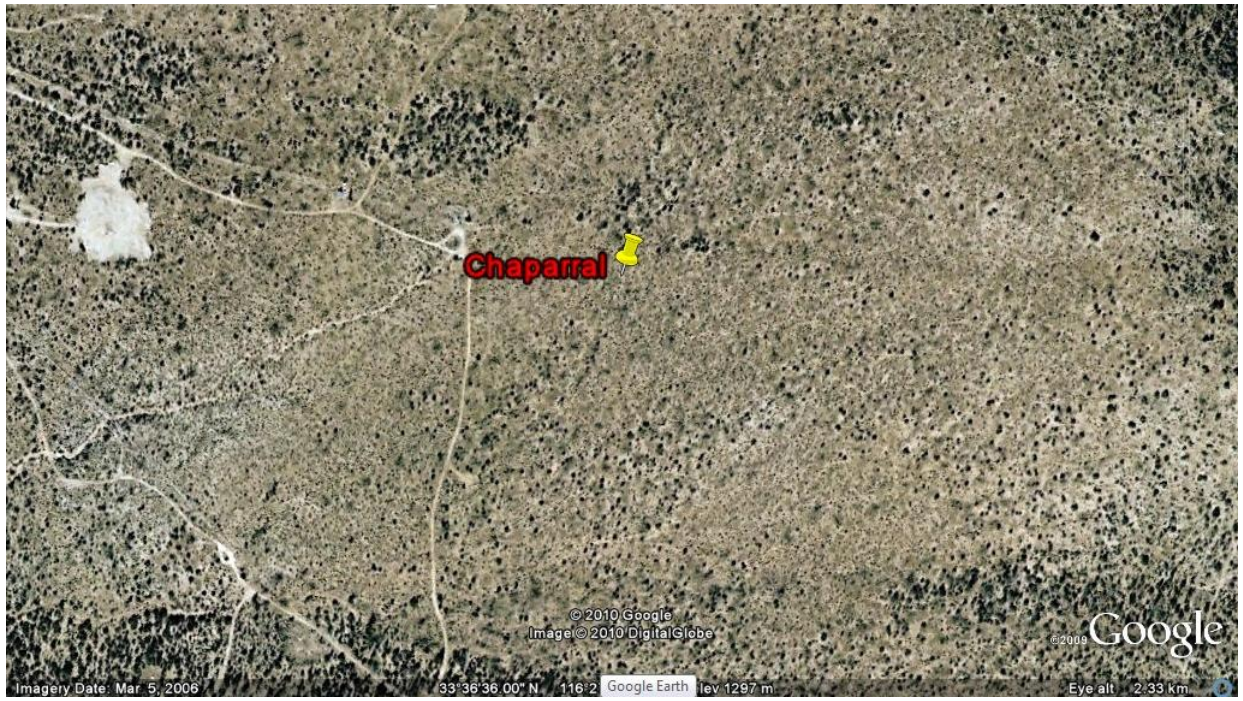


Figure 3b: Chaparral site.



Figure 3c: Desert site.



Figure 3d: Grassland and Sage sites.

2.2.2 Satellite Data

Six Landsat 5 TM images (path 40, row 37) taken on 4 April, 6 May, 23 June, 9 July, 10 August and 11 September of 2007 were examined in this heat budget analysis. The 6 May 2007 image is shown Figure 4. The image dates were chosen for cloud free conditions. Topographic data come from the shuttle radar topography mission (SRTM) digital elevation model (DEM) (Figures 5 and 6).

Southern CA Ameriflux tower sites

RGB-742 (5-6-2007)

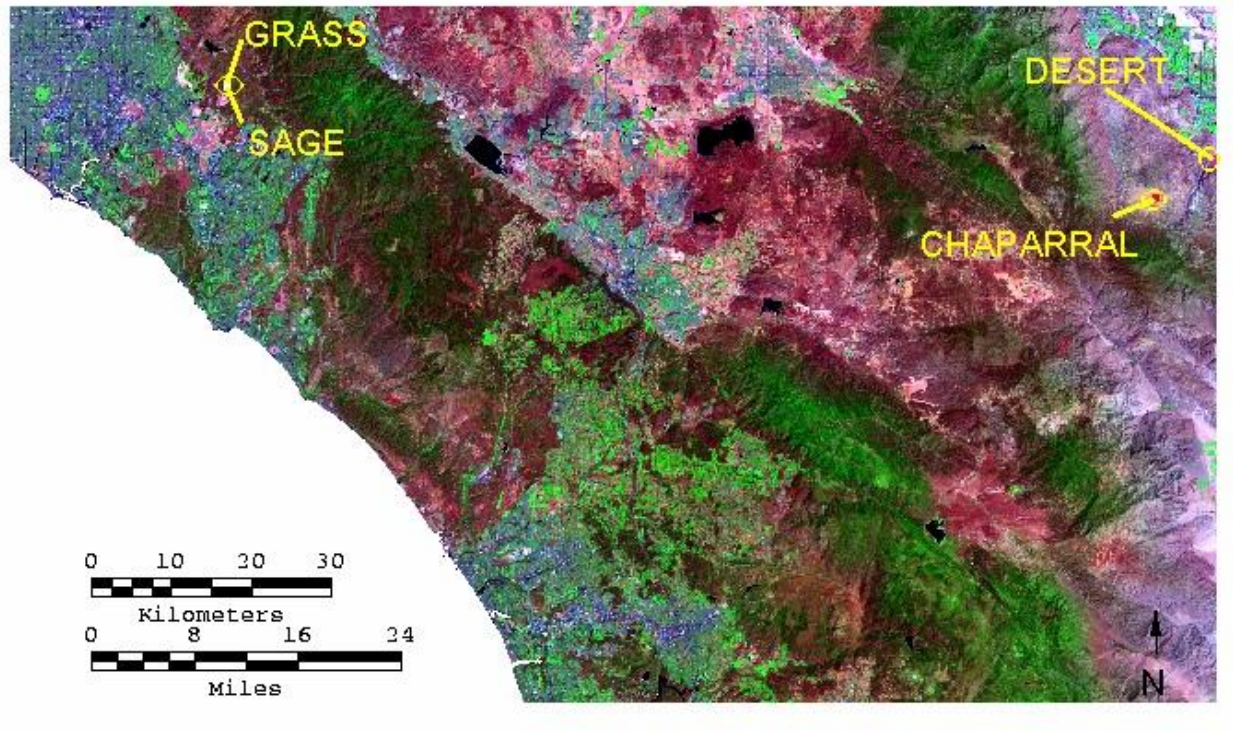


Figure 4: RGB-742 Landsat-5 TM image with flux tower locations from 6 May, 2007.

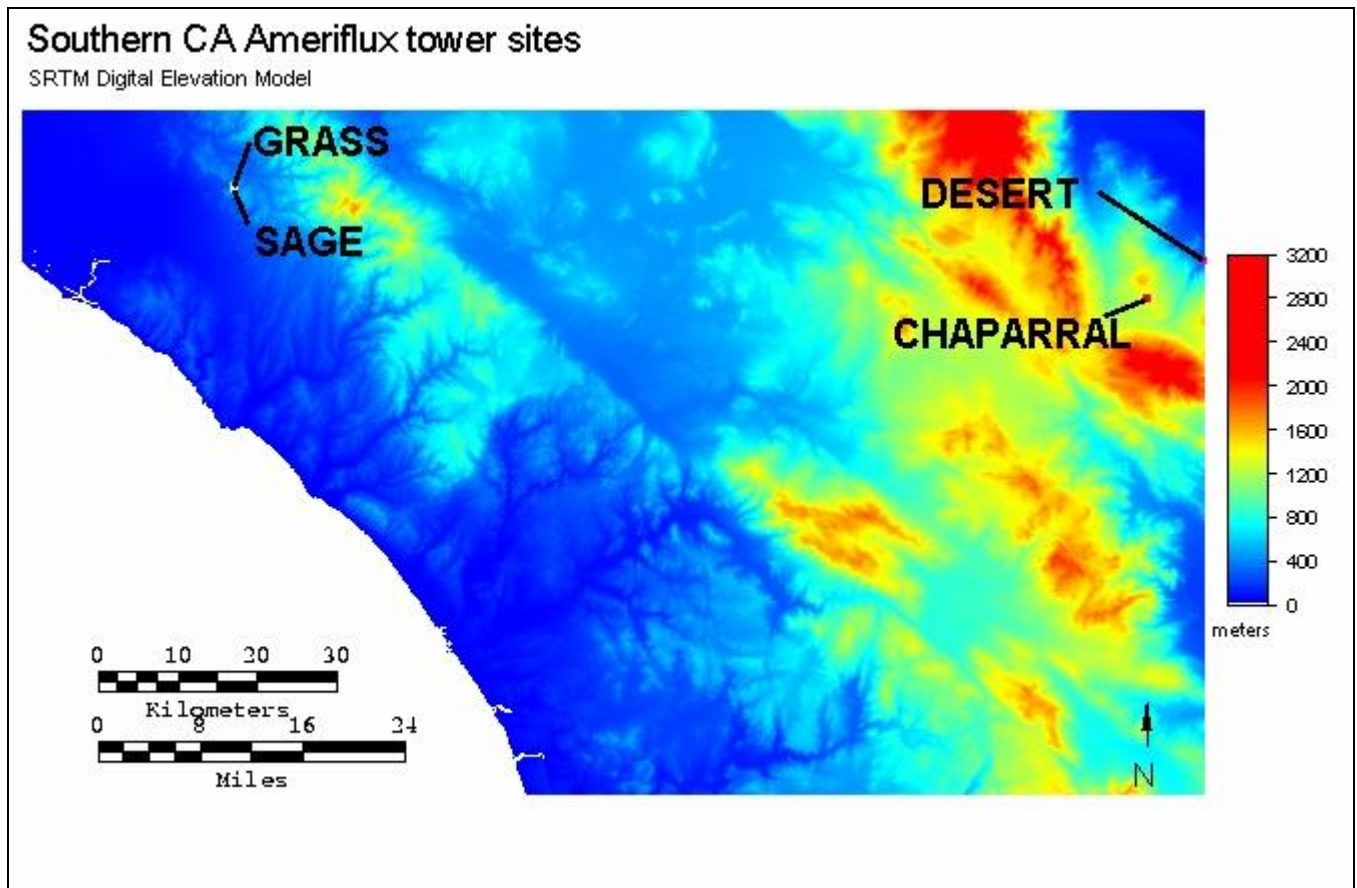


Figure 5: Shuttle Radar Topography Mission Digital Elevation Model. Elevation ranges from sea level to approximately 3000 m.

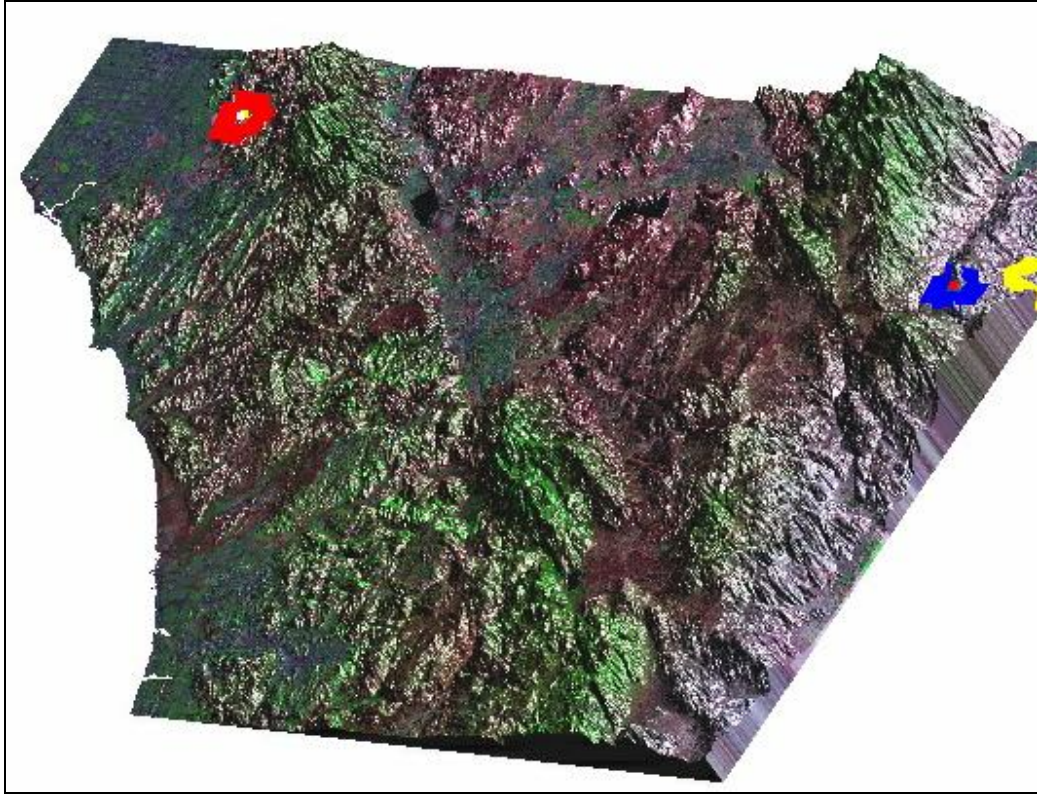


Figure 6: RGB-742 Landsat-5 TM image from May 6, 2007 draped over DEM. The red square indicates the location of the Grass and Sage sites, the blue square indicates the location of the Chaparral site and the yellow square indicates the location of the Desert site.

The satellite data are preprocessed to convert the raw digital number (DN) values of the individual pixels to reflectance and surface temperature (Appendix B). The Landsat-5 TM satellite provides seven bands of spectral radiance in the electromagnetic spectrum. Three bands are for visible light (bands 1, 2 and 3), three bands are for the near- and mid-infrared (bands 4, 5 and 7), and one band is for the thermal infrared (band 6). DN values for the visible and infrared bands are converted into spectral radiance and then reflectance using the corresponding calibration constants and solar position angles. Similarly, the thermal infrared band is converted from DN values to spectral radiance and then to brightness temperature. With these ground and satellite data, we calculate the surface heat budget for these images at the flux tower sites.

2.3 Surface heat budget

This study employs a simplified surface heat budget, which consists of the sum of the outgoing and incoming radiation at the Earth's surface (Figure 1)¹. Figures 7 and 8 illustrate our use of the satellite and the flux tower data to calculate the heat budget.

2.3.1 Incoming Solar Radiation

The total incident solar contribution can either be measured directly by the flux towers using a pyranometer or estimated using the solar zenith angle and an estimate of the atmospheric transmissivity (Figure 9). The two measures of insolation are defined as S1 and S2, respectively (Appendix A). S1 is measured by the tower and S2 is calculated as

$$S2 = S_0 * \cos(\theta_s) * t_o , \quad (1)$$

where S_0 is the solar constant, θ_s is the solar zenith angle, and t_o is atmospheric transmissivity. Liou (2002) prescribes a clear day transmissivity value of 0.75. However, it is important to note that the transmissivity varies widely with weather conditions.

2.3.2 Albedo

Using the flux tower data and the Landsat reflectance bands, three methods are investigated to calculate the albedo. One is a simple ratio of the incoming and reflected solar radiation as measured by the flux tower (a1). Another method (a2) is a weighted average of the Landsat reflective bands, using weights provided by Tasumi et al. (2008), and the third (a3) is a simple average of the six reflective Landsat bands (Appendix A, B):

$$a1 = \frac{\text{reflected (tower)}}{\text{incoming (tower)}} \quad (2a)$$

$$a2 = 0.254\rho_1 + 0.149\rho_2 + 0.147\rho_3 + 0.311\rho_4 + 0.103\rho_5 + 0.036\rho_7 \quad (2b)$$

$$a3 = \frac{\rho_1 + \rho_2 + \rho_3 + \rho_4 + \rho_5 + \rho_7}{6} , \quad (2c)$$

¹ In this section, each term of the heat budget is indicated by an alphabetical letter. The number following the letter indicates a particular method used to calculate that heat budget term.

where, ρ is the planetary reflectance for the i^{th} band (Figure 10).

2.3.3 Absorbed Solar Radiation

This study examines three methods of calculating the amount of solar radiation absorbed by the surface:

$$B = S * (1 - a), \quad (3)$$

where B is the amount of absorbed solar radiation, S is the incoming solar radiation, and a is the albedo. One measure of the absorbed solar radiation is derived completely from the flux towers using S_1 and a_1 (B1). The other methods use only satellite data, combining S_2 and a_2 (B2) or S_2 and a_3 (B3) (Appendix A).

2.3.4 Long-Wave Fluxes

The upward long-wave emission from the surface is calculated using

$$RS = \varepsilon_s \sigma T_s^4, \quad (4)$$

where ε_s is the surface emissivity, σ is the Stefan-Boltzmann constant, and T_s is the satellite-derived temperature of the surface (Figure 11, Appendix A). The value used for surface emissivity (0.95) is the average emissivity of bare, dry soils, dry vegetation and rock, which is characteristic of this area (Lillisand, 2004; Malek and Bingham, 1997).

The downward long-wave atmospheric emission was similarly found by

$$RA = \varepsilon_A \sigma T_A^4, \quad (5)$$

where ε_A is the atmospheric emissivity, σ is the Stefan-Boltzmann constant, and T_A is the near-surface atmospheric temperature, provided by the flux tower. In this study, it is assumed that the average atmospheric emissivity is approximately 0.67. However, it is important to note that this parameter varies with elevation and is dependent upon water vapor pressure (Staley and Jurica, 1972; Brutsaert, 1975; Malek, 1997). It is also assumed that all the downward long-wave radiation is absorbed by the surface, when in fact approximately 5% of the incoming long-wave radiation is reflected (Liou, 2002).

2.3.5 Net Radiation

There are three ways to measure the net radiation. The towers themselves can measure this term directly (RN1). The other two methods are derived using B2 (the amount of solar radiation absorbed using a2, RN2), or derived using B3 (the amount of absorbed solar radiation using a3, RN3) (Figure 12, Appendix A).

$$RN2 = B2 - RS + RA \quad (6a)$$

$$RN3 = B3 - RS + RA \quad (6b)$$

2.3.6 Turbulent Fluxes

The sensible and latent heat fluxes measured by the flux towers, defined as H and L respectively, are calculated using the eddy covariance method (Figure 13, Appendix A). These fluxes are calculated as

$$H = \bar{\rho}_a * \bar{C}_p * \overline{w'T'} \quad (7a)$$

$$L = -\bar{\rho}_a * l * \overline{w'q'} , \quad (7b)$$

where $\bar{\rho}_a$ is the air density, C_p is the specific heat, w is the vertical velocity, l is the latent heat of water, T_A is the temperature and q is the specific humidity. The primes represent the perturbations and the bars represent 30 minute mean values.

2.3.7 Imbalance

By combining the net radiation and turbulent flux terms, the general simplified heat budget equation can be written as

$$G = RN - H - L \quad (8)$$

where G is the ground heat storage flux, or the imbalance. Since the flux tower data do not provide a measure of the ground storage flux, and it cannot be estimated from satellite data (Malek and Bingham, 1997; Tanaka *et al.*, 2001), this term is computed as the residual. When the right side of equation (8) is positive, the surface heat budget has an excess incoming heat flux. When the right side is negative, the surface heat budget has an excess outgoing heat. Three different imbalance terms are examined using the three different net radiation values defined above (Figure 14, Appendix A).

$$G1 = RN1 - H - L \quad (9a)$$

$$G2 = RN2 - H - L \quad (9b)$$

$$G3 = RN3 - H - L \quad (9c)$$

Using equations 1-9, the individual terms of the surface heat budget are obtained using either ground data or a combination of ground and satellite data. Comparisons between the various methods of estimating the surface heat budget allow us to determine what satellite and ground data offer to surface heat budget studies. The heat budget calculation methods are also compared by date and site to determine whether these estimates provide indications of an albedo or latent heat feedback over the course of the season and whether it is possible to detect changes between land cover types.

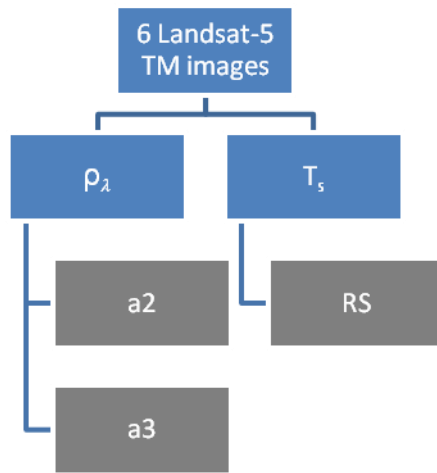


Figure 7: Flow chart of heat budget terms (equations 1-9, Appendix A) derived from the Landsat-5 TM images. The Landsat-5TM satellite provides reflectance values for each band, which are used to calculate a2, a3. The satellite also provides radiance values which are used to estimate T_s and thus RS.

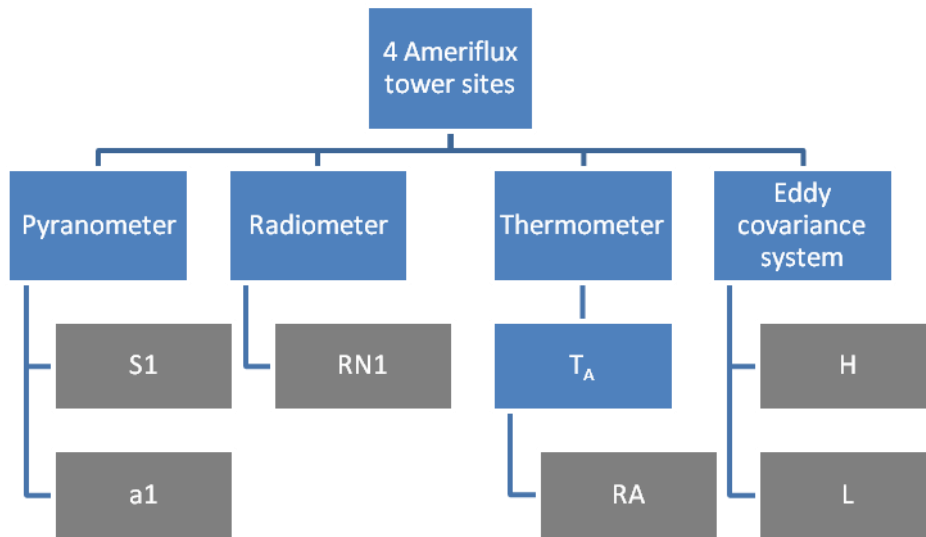


Figure 8: Flow chart of heat budget terms (equations 1-9, Appendix A) derived from the Ameriflux tower data. The Ameriflux sites have a pyranometer which measures S_1 and is used to calculate a_1 . The Ameriflux radiometer measured RN_1 . The towers' thermometers measure T_A , which is used to estimate RA . The eddy covariance system measure H and L .

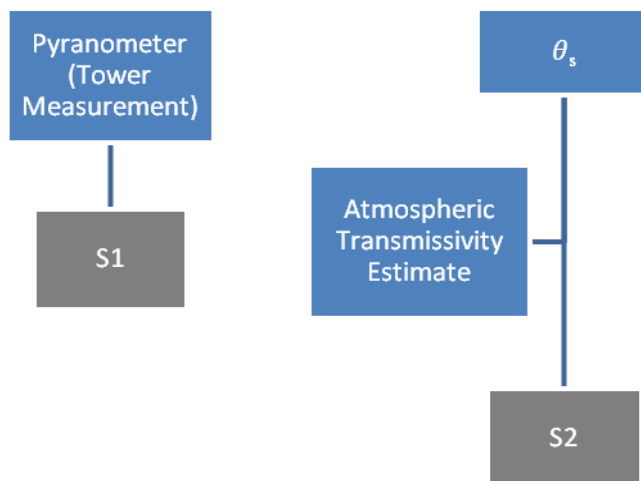


Figure 9: Flow chart of the two methods examined for the incoming solar radiation (equation 1, Appendix A). S_1 is measured by the pyranometer from the tower. S_2 is calculated from the solar zenith angle and an estimate of the atmospheric transmissivity.

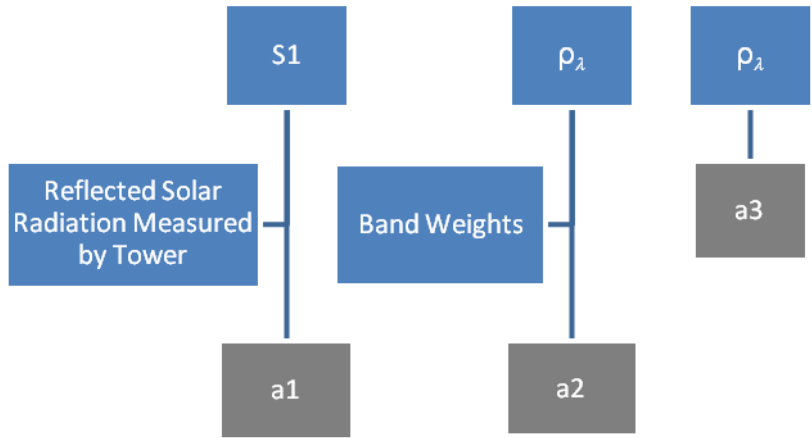


Figure 10: Flow chart of the three methods examined for albedo (equation 2, Appendix A). a1 is estimated from S1 and the reflected radiation, both of which are measured by the tower. a2 is estimated from the band reflectances and band weights. a3 is estimated from the band reflectances.

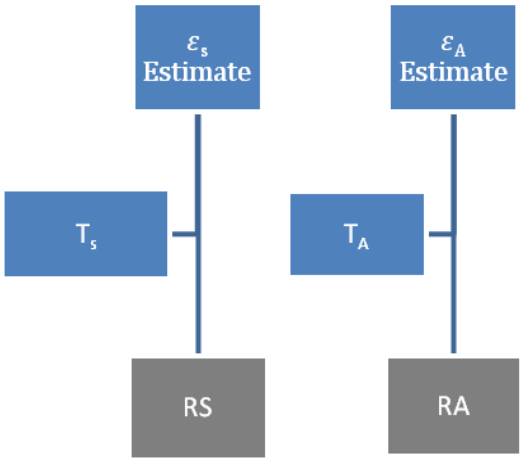


Figure 11: Flow chart of the long-wave fluxes from the surface and atmosphere (equations 4-5, Appendix A). RS is calculated from the surface temperature and an estimate of the surface emissivity. RA is calculated from the air temperature and an estimate of the atmospheric emissivity.

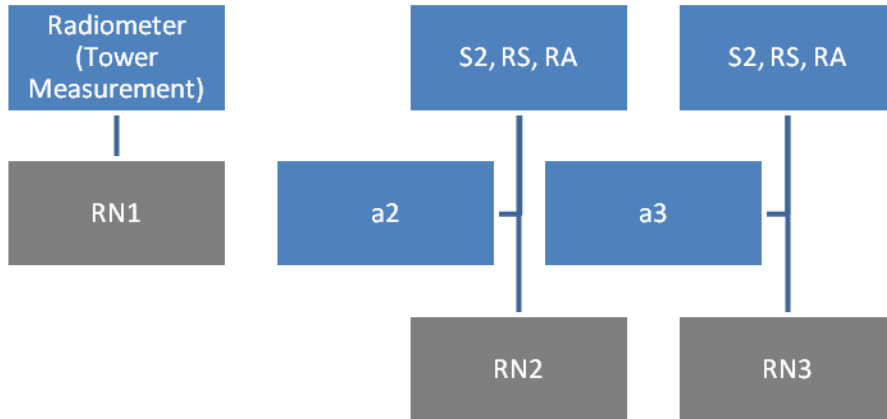


Figure 12: Flow chart of the three methods for the net radiation (equation 6, Appendix A). RN1 is measured by the tower. RN2 is calculated from S2, RS, RA, and s2. RN3 is calculated from S2, RS, RA, and a3.

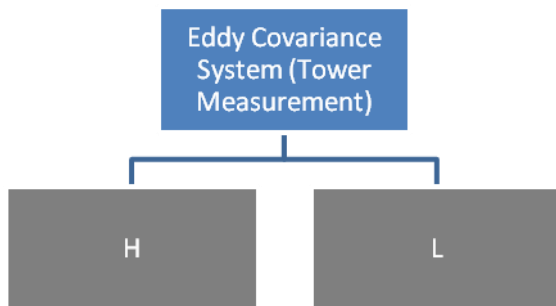


Figure 13: Flow chart for the turbulent heat fluxes (equation 7, Appendix A). Both H and L are measured by the tower.

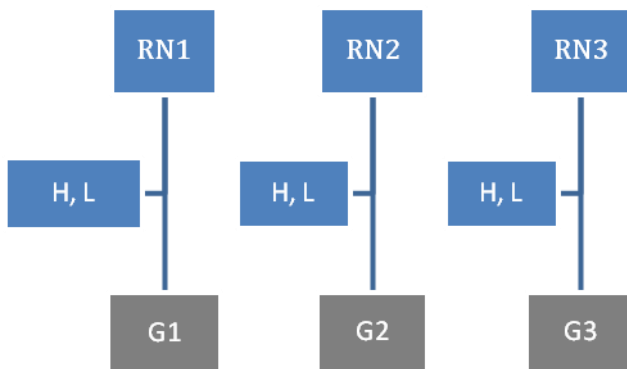


Figure 14: Flow chart of the three methods for the ground heat storage (equations 8-9, Appendix A). G1 is estimated from RN1, H, and L. G2 is estimated from RN2, H, and L. G3 is estimated from RN3, H, and L.

3 Results

The heat budget terms are calculated for each of the four sites and six image dates using the various methods described in the previous section (equations 1-9, Figures 7-14, Appendix A). They are discussed in three portions. The first compares the different methods for calculating the terms of the surface heat budget by averaging over the sites and dates. In the second portion, the terms for each date are averaged over the sites and methods to investigate the evolution of the heat budget over time. Finally, in an effort to detect trends in the budget according to land cover type, the heat budget terms are averaged over time and method for each site.

3.1 All Sites and All Dates

To display the general nature of the summer heat budget in Southern California, each term is averaged for all dates, sites and methods (Figure 15). The average incoming solar irradiance is approximately 810 W/m^2 , while the average reflected solar irradiance is approximately 100 W/m^2 . The average emitted irradiance from the surface is approximately 480 W/m^2 and the average incoming atmospheric irradiance is approximately 280 W/m^2 . These four terms contribute to the net radiation which has an average value of approximately 510 W/m^2 , similar to the net radiation value found in similar studies done by Tanaka et al. (2001) and Malek and Bingham (1997). The average turbulent sensible heat flux is approximately 250 W/m^2 and the average turbulent latent heat flux is

approximately 30 W/m^2 . Altogether this gives an average residual ground heat flux of approximately 230 W/m^2 , which is also similar to the value found by Tanaka et al. (2001) during this time of day (approximately 9:30am). It is important to note that many of the heat budget terms have large spreads in the values about their respective means (Table 3). The following sections discussing temporal and locational trends (3.2 All dates, 3.3 All sites) investigate whether these large variations in the heat budget are due to seasonal changes, vegetation cover, or error.

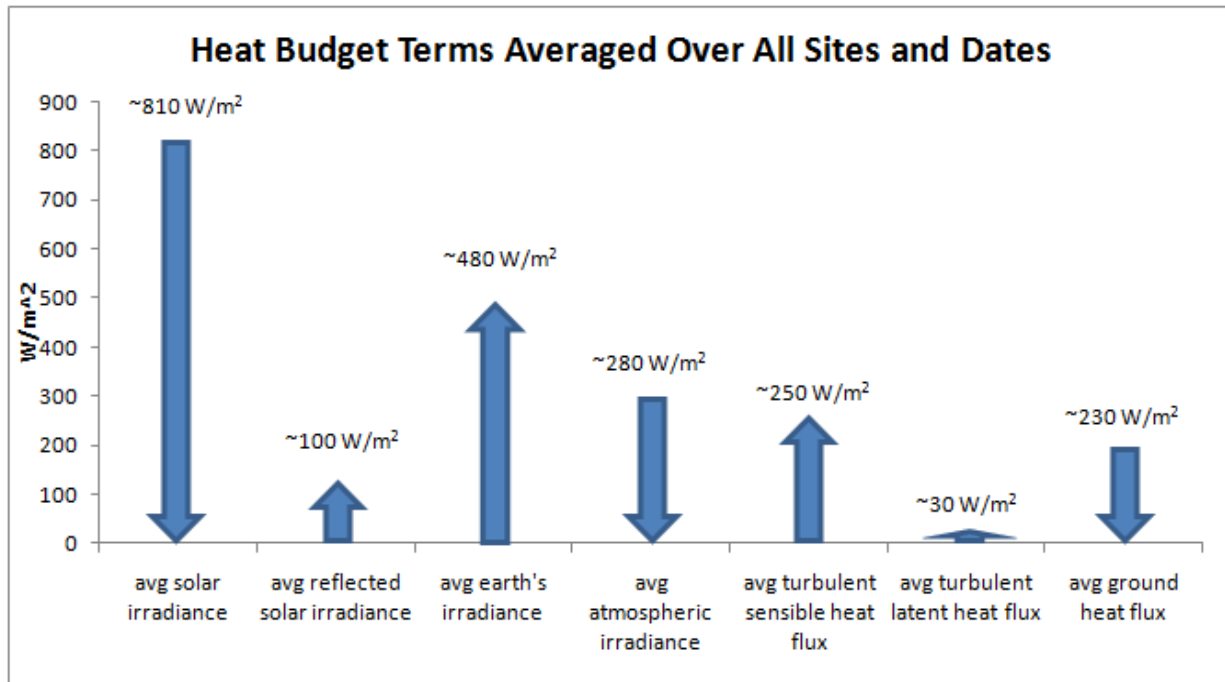


Figure 15: Heat budget terms averaged over all sites, dates and methods

Heat Budget Term	Average Value (W/m^2)	Spread of Values as a Percentage of the Mean Value
solar irradiance	809	14%
reflected solar irradiance	113	38%
earth's irradiance	481	7%
atmospheric irradiance	275	2%
turbulent sensible heat flux	247	43%
turbulent latent heat flux	29	125%
ground heat flux	226	73%

Table 3: Heat budget terms averaged over all sites, dates, and methods

In order to compare the various methods of calculating the surface heat budget, each component is averaged over all sites and all dates, and the results for the different methods are plotted side-by-side (Figure 16). The two measurements of incoming solar radiation (S1 and S2) differ by 18%. This disagreement may be due to either instrumental error in S1, or error in the estimate of the atmospheric transmissivity in S2. The later is the likely source of disagreement between the two methods. The following sections (3.2 and 3.3) show that there were a couple days with hazy atmospheric conditions, lowering the measured insolation (S1). This is similarly true for the absorbed solar radiation measurements (B1, B2, B3). The absorbed solar radiation, as estimated from the flux tower data (B1), is much smaller than the absorbed solar radiation as estimated from the satellite data (B2, B3). B1 differs from B2 and B3 by approximately 26%, while B2 and B3 differ by approximately 1%. The three measures of net radiation (RN1, RN2, RN3) are also in disagreement. RN1 differs from RN2 and RN3 by approximately 28%, while RN2 and RN3 differ by approximately 1%. All three albedo methods (a1, a2, a3) produce similar values between 0.15 and 0.20. None of the different albedo methods differ by more than 12%. As is shown in Figures 15 and 16, the outgoing long-wave radiation from the surface (RS) is approximately 480 W/m^2 , the incoming atmospheric long-wave radiation (RA) is approximately 300 W/m^2 , the sensible heat flux (H) is approximately 260 W/m^2 and the latent heat flux (L) is approximately 10 W/m^2 . The three ground storage values (G1, G2, G3) are all within the range of values expected for this term according to a similar study done by Tanaka et al. (2001). The disagreement between the measurements of incoming solar radiation propagates down to the estimations of the ground storage flux methods; G1 differs from G2 and G3 by approximately 73%, while G2 and G3 differ by approximately 3%.

To further compare the various methods, we plotted the heat budget terms for all sites and dates calculated using the ground based data against those calculated from satellite data (Figure 17). There appears to be no correlation between the tower measurement (S1) and the calculated estimate (S2) for incoming solar radiation (R^2 value less than 0.25). The small variability in S2 arises from using the same transmissivity for all sites and dates and the same solar zenith angle for all sites. Only the tower data, if it is accurate, would detect variations in transmissivity by site and date.

Unlike other studies (Tanaka et al, 2001; Xu and Haginoya, 2001; Ma et al., 2002, 2003, 2004, 2006) we do not observe good agreement between the measurement-based and the derived albedo, absorbed solar radiation, net radiation, or ground storage flux. Figure 16 suggests that a3 may agree well with the tower measurement of the albedo (a1); however, Figure 17 illustrates that neither a2 nor

a3 are well correlated with a1. The weak relationship between the ground and satellite estimations of albedo may stem from the fact that the tower measures the surface reflectance, while satellites measure the reflectance at the top of the atmosphere. Future satellite estimates of albedo should include atmospheric corrections, such as dark object subtraction, in order to account for the atmospheric transmissivity. Another source of disagreement may be caused by the larger satellite pixel area. The towers measure the reflectance at for a smaller spatial area, while the satellite averages the reflectance over 30 m x 30 m pixels. The satellite data may provide a better estimate because the larger footprint is closer to the tower footprint used for the turbulent flux (Gash, 1986; Wang et al., 2006).

In contrast, we do observe a strong linear correlation between the satellite methods for albedo (a2, a3), absorbed solar radiation (B2, B3), net radiation (RN2, RN3), and ground storage flux (G2, G3), as shown in Figure 17. This is encouraging as it illustrates consistency between the two satellite methods' algorithms. a2 and a3 give similar albedo values for areas of a certain cover type.

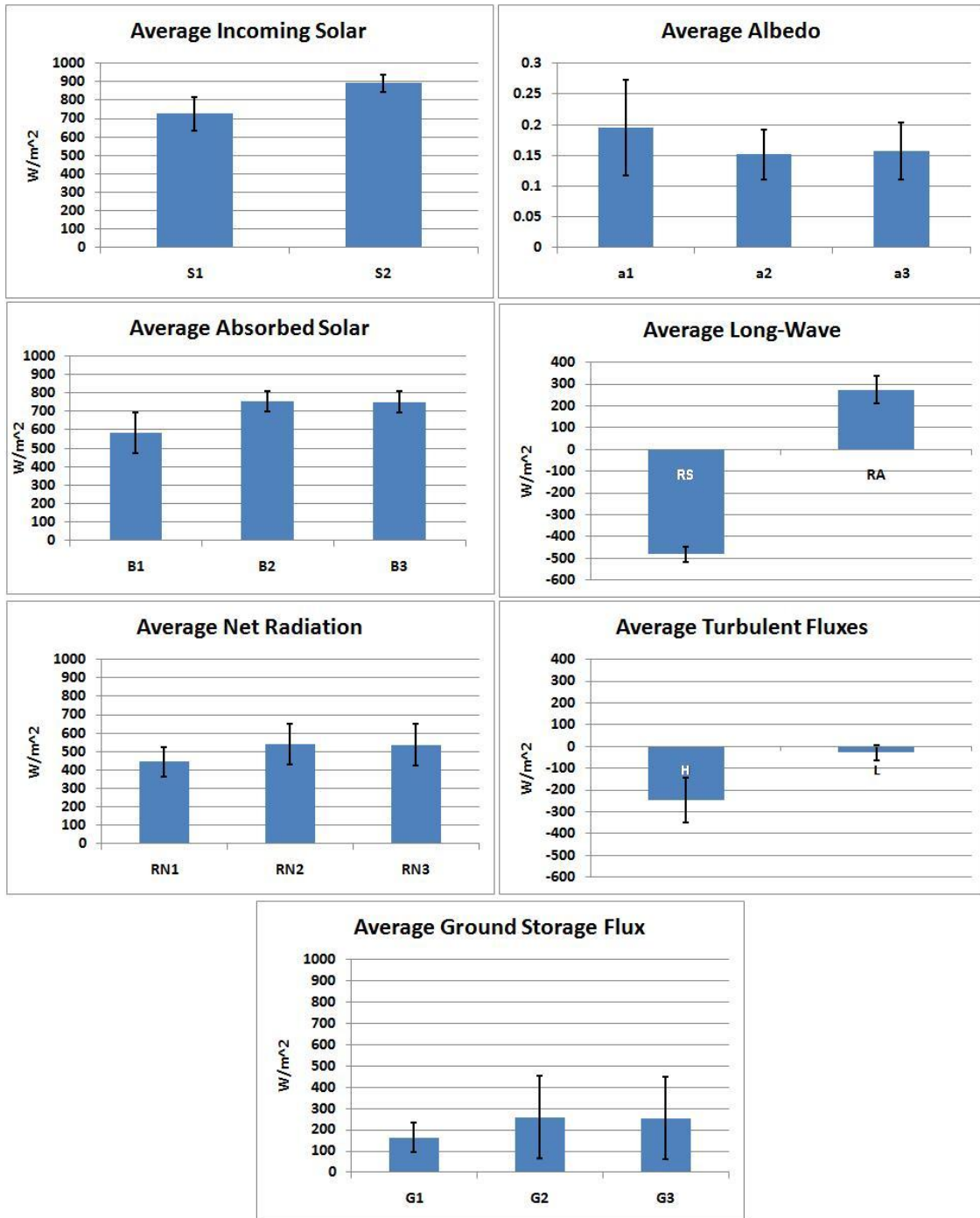


Figure 16: Comparison of different methods for calculating heat budget terms (averaged over all sites and dates). Error bars indicate variation about the mean values.

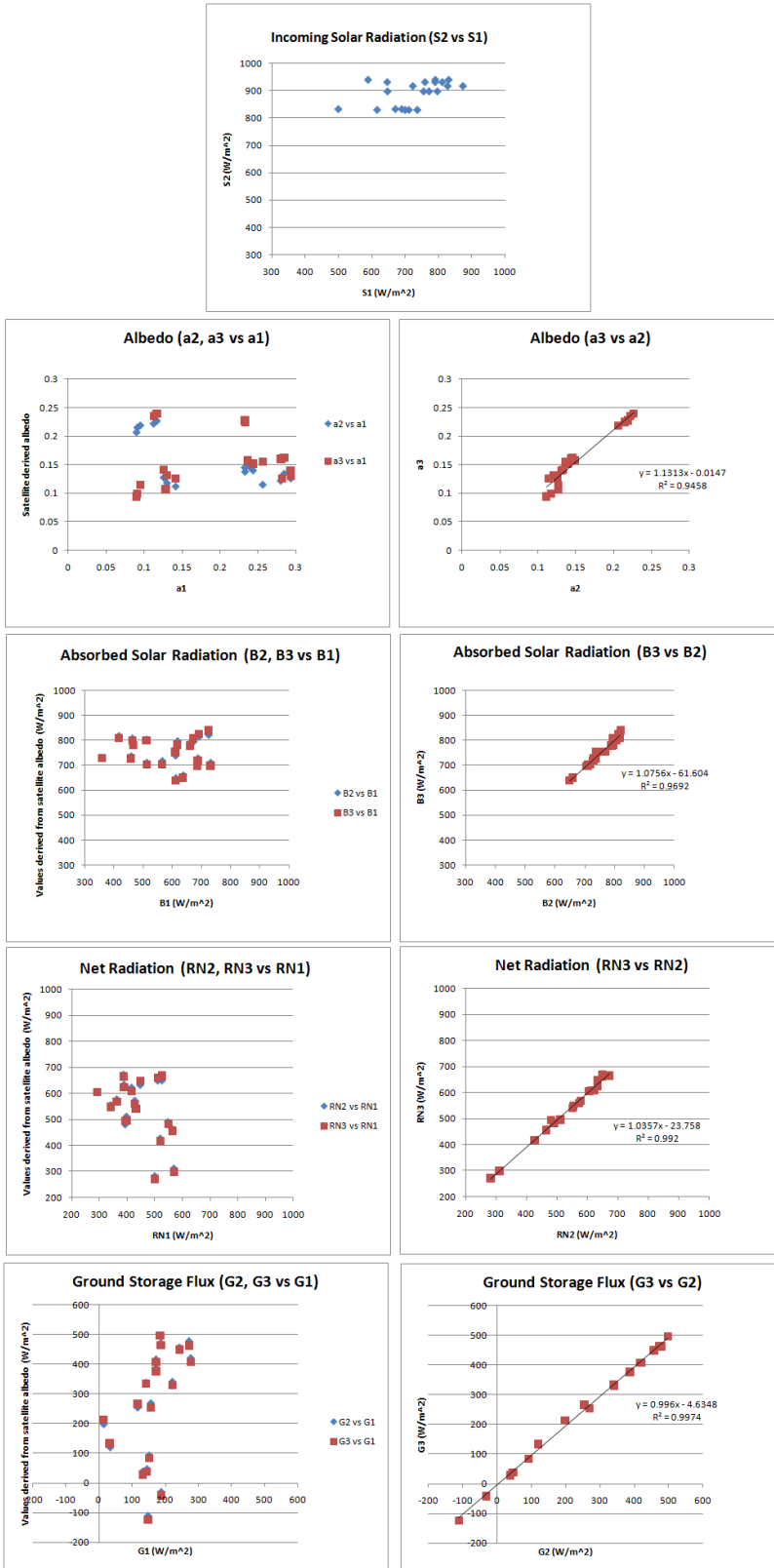


Figure 17: Correlation between methods

3.2 Trends by Date

To determine temporal changes over Southern CA summer, each term of the heat budget for each date is averaged over the four sites (Figure 18). As expected, the incoming solar radiation has a significant seasonal signal for both S1 and S2 methods. The S2 method reaches a peak of approximately 940 W/m^2 in June, the month of the summer solstice. However, the S1 method peaks with a value of approximately 810 W/m^2 in the earlier month of May. The low June S1 value is probably due to a high transmissivity on that day. The tower data indicate that all the sites have somewhat reduced insolation values on that date. In contrast to this significant seasonal pattern in the amount of solar radiation reaching the surface, the albedo varies very little over time for all three methods. a1, a2 and a3 all vary by less than 7% about their respective means and with no distinct pattern. The a1 method gives a slightly higher value than the a2 and a3 methods (the mean values of a1, a2 and a3 are approximately 0.19, 0.15 and 0.16 respectively). a1 differs from a2 and a3 by approximately 19%, while a2 and a3 differ by approximately 3%. It is important to note that the a1 method, which is derived from flux tower data, is an average over a small instrumental field of view. The a2 and a3 methods, which are derived from the satellite data, are averaged over large $30 \text{ m} \times 30 \text{ m}$ pixel areas. The flux tower footprint, which is a measure of the surface area that influences the vertical turbulent flux in tower eddy covariance methods, is approximately 1 km^2 , or approximately $30^2 = 900$ pixels (Wang et al., 2006). The satellite covers more surface than the downward facing pyranometer, and potentially captures a more comprehensive view of the complex surface at a particular location.

The overall trend in the absorbed radiation follows a similar pattern. The methods that estimate the absorbed solar radiation from S2 and a2 or a3 (B2, B3) reach their highest values in June (approximately 790 W/m^2), while the method that estimates the absorbed solar radiation from S1 and a1 (B1) reaches its highest value in May (approximately 650 W/m^2). This may be due to a slightly elevated a1 value in June (a1 is approximately 0.21 in June, 0.19 before June, and 0.18 after June). The net radiation also follows a similar pattern to the incoming solar radiation. RN1 reaches a maximum of approximately 480 W/m^2 in May, while RN2 and RN3 reach a peak of approximately 600 W/m^2 in June. The RN1 method has an unusually low value in June (approximately 300 W/m^2), possible due to instrumental error or hazy atmospheric conditions.

Over the course of the season there is a very slight increase (less than 70 W/m^2) in both the surface and atmospheric long-wave fluxes (RS, RA), which arises from the increase in surface and air

temperature (both increase by approximately 10°C). There does not appear to be any strong seasonal variation in the latent heat flux (L). It varies quite a bit over time (by approximately 100% about the mean), but with no discernible pattern and generally has very small values (less than 100 W/m^2). However, the sensible heat flux (H) does appear to have a seasonal pattern, which may be tied with the variation in the incoming solar radiation (Figure 19-20). The sensible heat flux increases and decreases in magnitude as the solar radiation intensifies then subsides over the course of the season. When the insolation is at its highest value during the solstice, the sensible heat flux is also large. Before and after the solstice when the insolation is not as high, the sensible heat flux is reduced as well. Overall, the budget shows no sign of seasonal drying, nor any indication of an albedo or latent heat feedback.

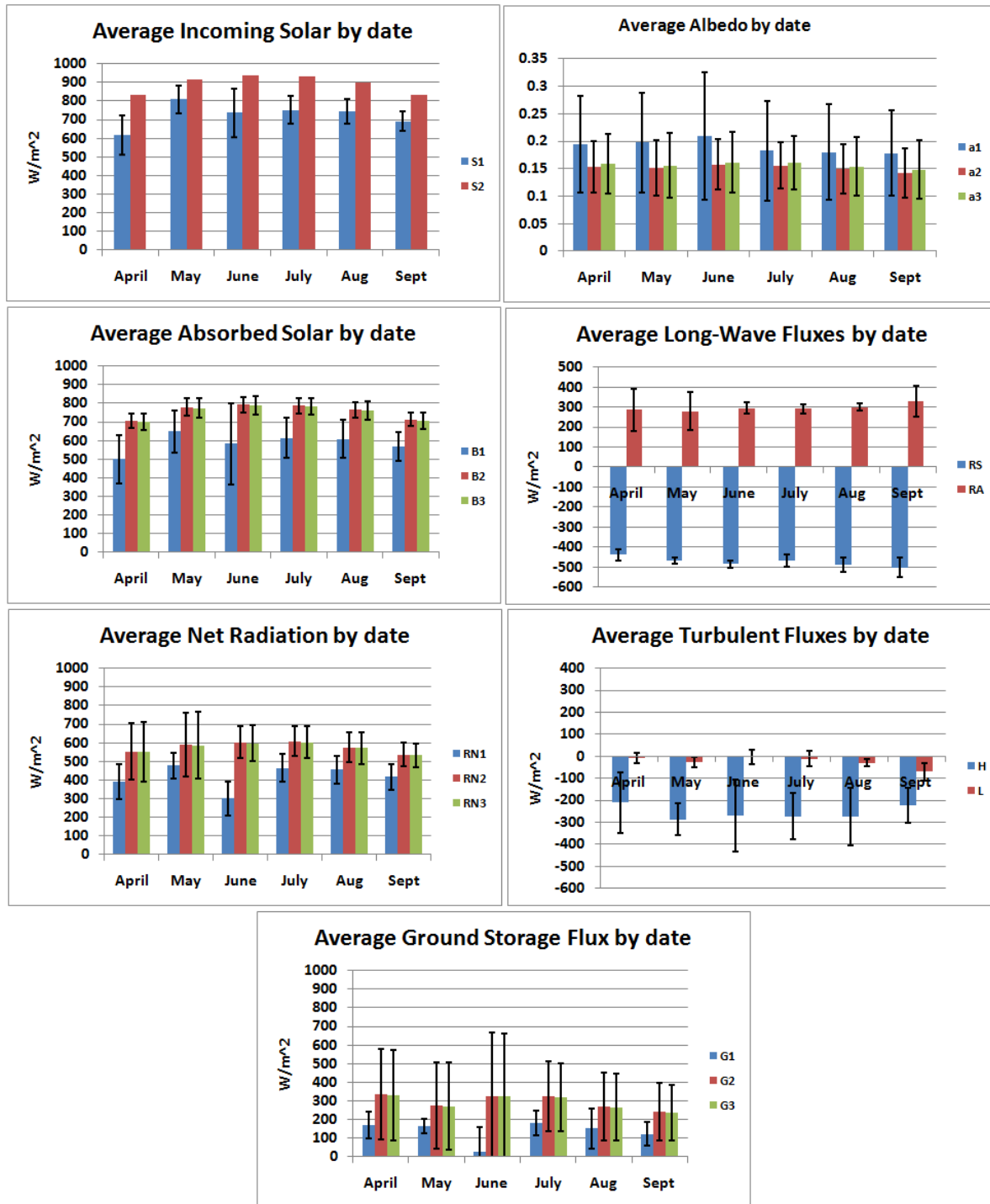


Figure 18: Temporal heat budget trends (April 4, May 26, June 23, July 9, August 10 and September 11 of 2007 at 9:30 local time). Error bars indicate variation about the mean date values.

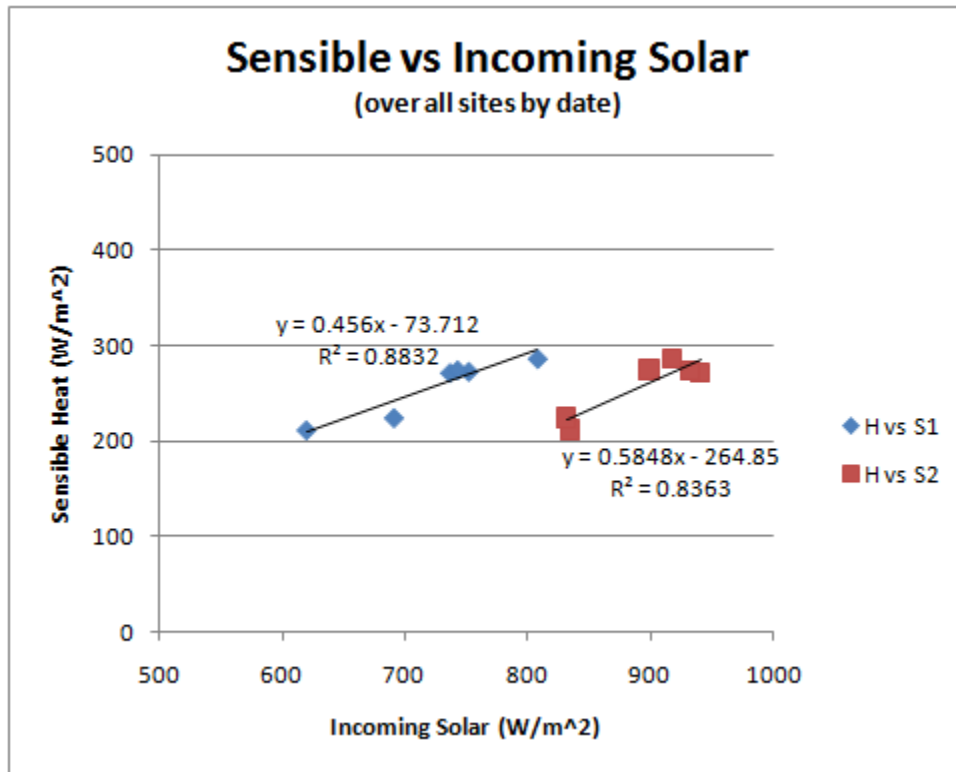


Figure 19: Sensible heat flux versus insolation.

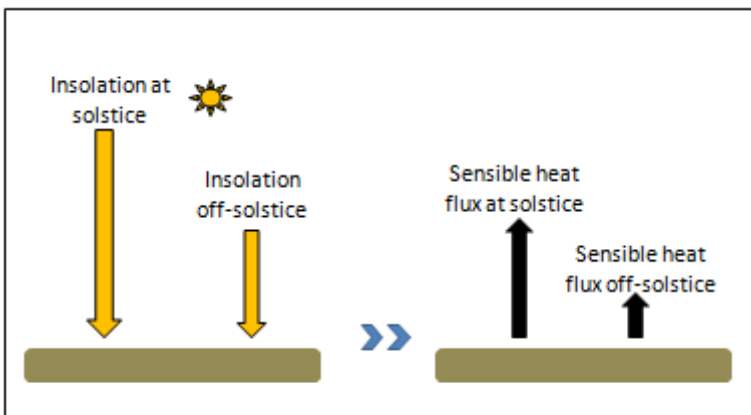


Figure 20: Illustration of the dominant seasonal relationship between insolation and sensible heat flux.

3.3 Trends by Site

To investigate variation in the heat budget between different land cover types, the terms of the heat budget are averaged over all dates for each site (Figure 21). All four Ameriflux tower sites are at similar latitudes and are located in areas with level terrain. The locational differences in longitude and

elevation are also small (Table 2). Except for the Desert site, which is located in an arid climate, all the Ameriflux towers examined in this study are located in semi-arid climates.

The amount of incoming solar radiation (S_1 , S_2) is similar for each site (S_1 and S_2 are approximately 730 W/m^2 and 890 W/m^2 respectively); however, the S_1 method gives an unexpectedly low insolation value at the Desert site (approximately 620 W/m^2). This could be due to either instrumental error or hazy atmospheric conditions, which are common in the area (COHA, 2004). The Desert site has a relatively low elevation (Table 2) and is surrounded by the San Bernardino Mountains to the north, the Santa Rosa Mountains to the south, the San Jacinto Mountains to the west, and the Little San Bernardino Mountains to the east. Wind transports pollutants from coastal urban areas such as Los Angeles to this isolated valley, creating smog at the tower location.

The Chaparral and Desert sites have significantly higher albedo values (approximately 0.25) than the Grass and Sage sites (approximately 0.13). This difference in albedo leads to higher values in the amount of absorbed solar radiation (B_1 , B_2 , B_3) and net radiation (RN_1 , RN_2 , RN_3) at the Grass and Sage sites. The Grass and Sage sites have an average absorbed solar radiation value of approximately 740 W/m^2 and an average net radiation value of approximately 550 W/m^2 . On the other hand, the Chaparral and Desert sites have an average absorbed solar radiation value of approximately 630 W/m^2 and an average net radiation value of approximately 450 W/m^2 . The low S_1 value for the Desert site is propagated into the estimate of the absorbed solar radiation (B_1) for this location. A very high albedo value (a_1) also contributes to the smaller amount of absorbed solar radiation (B_1 value of approximately 450 W/m^2) at the Desert site.

The surface and atmospheric long-wave radiation (RS , RA) are slightly elevated at the Chaparral and Desert sites (by approximately 40 W/m^2) and there is very little latent heat flux (L) across all the sites (less than 50 W/m^2), with the Desert site having the lowest value (approximately 3 W/m^2). The Grass and Sage sites have significantly higher sensible heat flux (H) than the Chaparral and Desert sites. The Grass and Sage sites have an average sensible heat flux of approximately 170 W/m^2 while the Chaparral and Desert sites have an average sensible heat flux of approximately 350 W/m^2 . Because the Chaparral and Desert sites have low latent and sensible heat flux terms, these locations have larger values for the ground storage flux (an average ground storage flux of approximately 270 W/m^2). Figure 6a-d and Appendix C indicate that the Grass and Sage sites have denser vegetation cover, which lowers albedo values and increases net radiation. In addition, Figures 22-24 illustrate the relationship between the albedo and ground heat flux. When albedo decreases, the sensible heat flux increases (Figure 22),

which in turn causes a decrease in the ground heat storage (Figure 23). Furthermore, the vegetation cover at these two sites possibly shades the surface, decreasing the ground heat storage. Vegetated surfaces tend to have cooler surfaces than those with no vegetation (Charney, 1975). The albedo and ground storage effects may be driving the large sensible heat flux values at these locations (Xue, 1996).

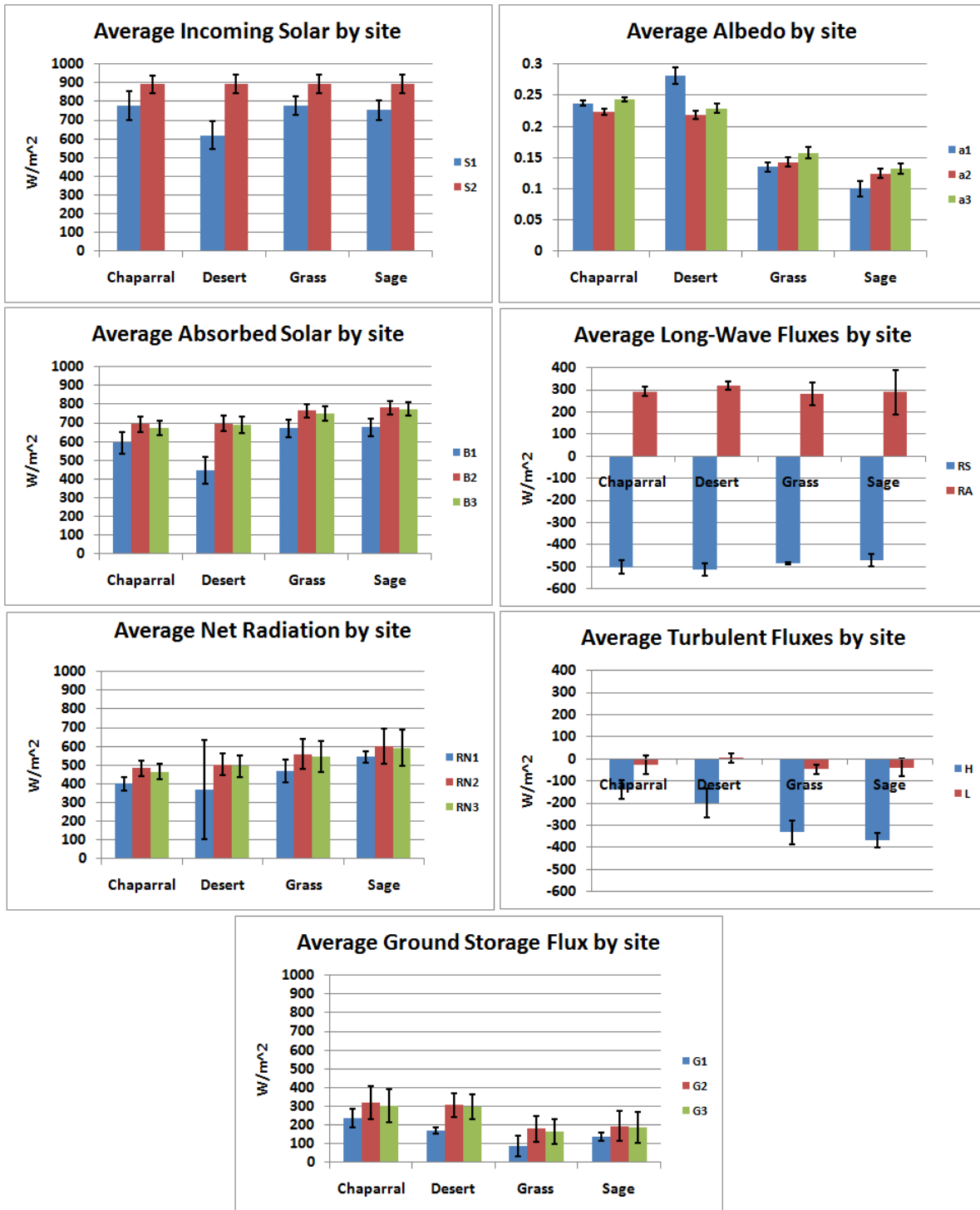


Figure 21: Heat budget terms grouped by site. Error bars indicate variation about the mean site values.

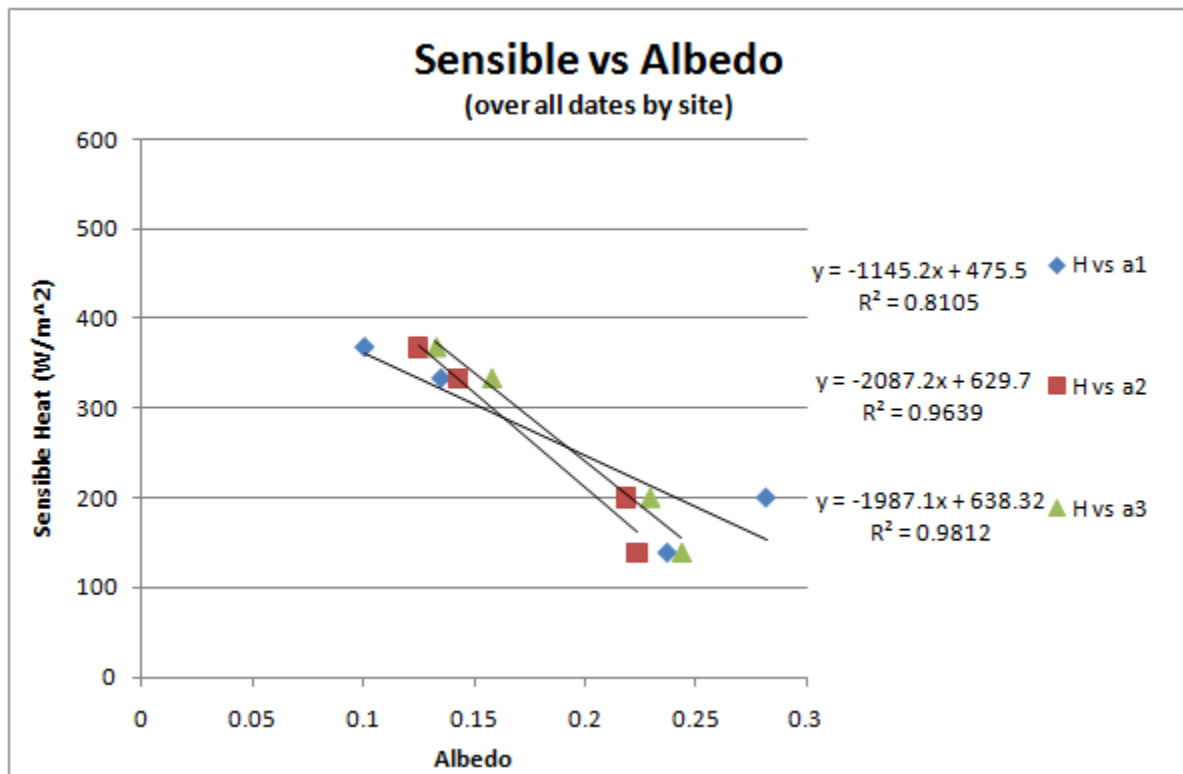


Figure 22: Sensible heat flux versus albedo.

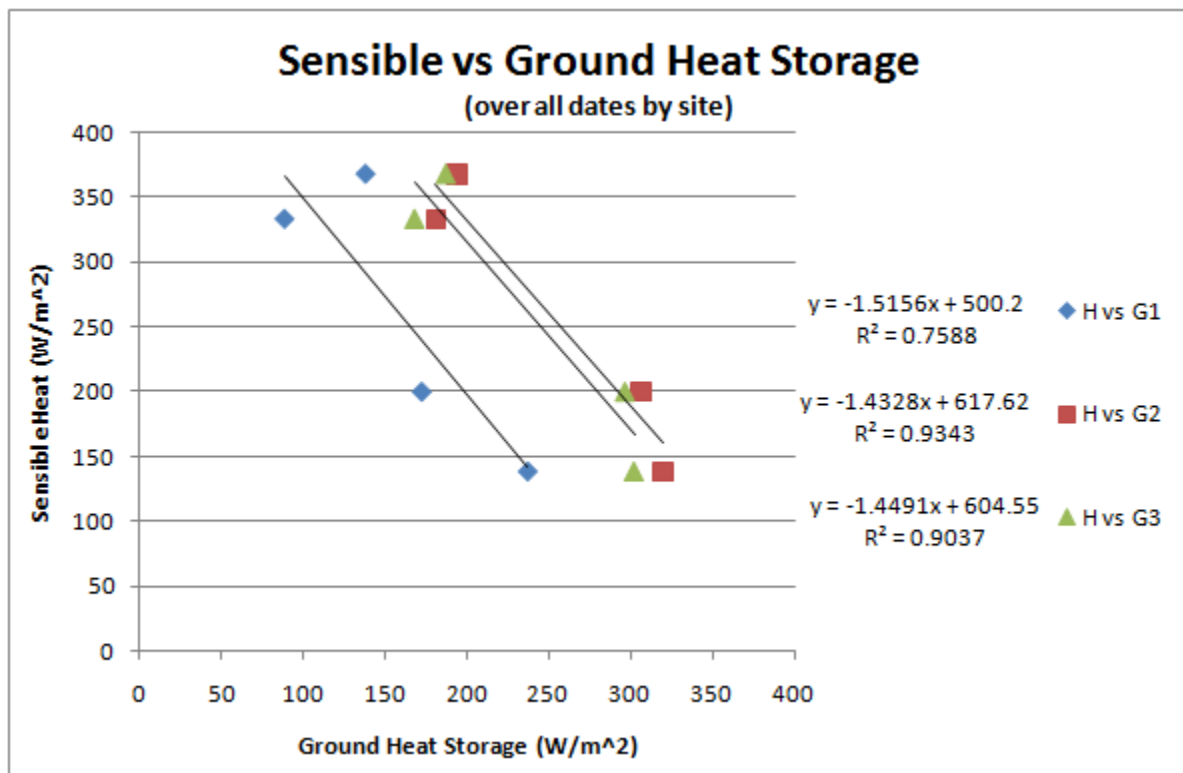


Figure 23: Ground heat storage versus sensible heat flux.

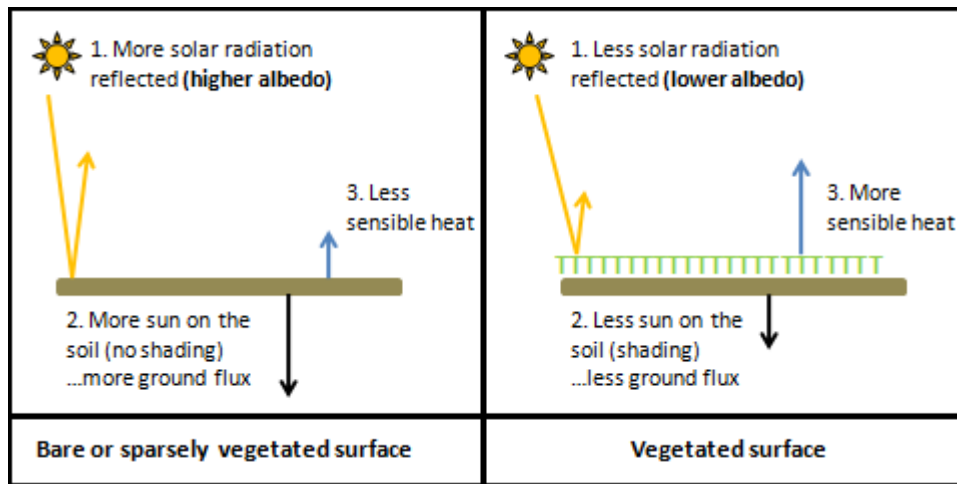


Figure 24: Interpretive illustration of the effect of vegetation on the ground flux and sensible heat.

4 Implications for Surface Feedbacks

Over the course of a typical summer in Southern CA, we expect to observe a decrease in NDVI (Normalized Difference Vegetation Index) and an increase in albedo as the vegetation becomes more stressed and therefore, brighter. The albedo feedback as described by Charney (1975) is typically found in desert regions, such as the African Sahel or Mongolia (Xue, 1996). This feedback is best observed under drought conditions and when there are significant changes in the vegetation cover in the area. However, we observe no strong changes in albedo over the summer despite decreases in NDVI (Figure 18 and 25). There is no strong correlation between the NDVI and albedo over time, though there is a strong relationship between sites (Figure 26). NDVI may be decreasing over the course of the season, indicating some changes in band reflectance; however, these changes are occurring in a manner that does not alter the albedo.

As the Southern CA region dries over the course of the season, there is less water available for evaporation. From this, we expect to observe a decrease in the latent heat flux as the season progresses. The latent heat or soil-moisture feedback is also best observed in drought conditions (Durre et al., 2000; Zaitchik et al., 2006). For example, during the 2003 European summer heat wave vegetation was greatly impacted by the lack of precipitation and elevated temperatures. The soil dried leading to a reduction in the latent heat flux and an increase in the sensible heat flux. It is possible to observe these feedbacks if there are anomalously high temperatures that severely affect vegetation.

Because Southern CA is an arid environment, there is little soil moisture and the latent heat flux is low year round. One would expect the albedo feedback dominate and rather than observe an increase in the sensible heat flux (Durre et al., 2000). However, as with albedo, we see no consistent decrease in the latent heat flux across the sites over time and we observe a strong increase in the sensible heat as the summer progresses, especially over bare surfaces (Figures 18-20). Similar results in the sensible heat were found by Xue (1996) with model studies of the Inner Mongolian Grasslands.

Our study does observe differences in the heat budget among the sites (Figures 21 and 24). A strong relationship exists between the sensible heat flux and albedo, where high values of sensible heat correspond with low albedo values (Figure 22). We also find that there is strong linear relationship between the sensible heat flux and ground heat storage (Figure 23). When the sensible heat flux is large, the ground heat flux is small. Figure 24 illustrates our interpretation as to how the albedo and ground heat flux work together to influence the sensible heat flux. Areas with little or no vegetation are more reflective. However, such bare surfaces have larger ground heat storage, which may be due to the lack of shading of the surface. These two effects combine to reduce the sensible heat flux.

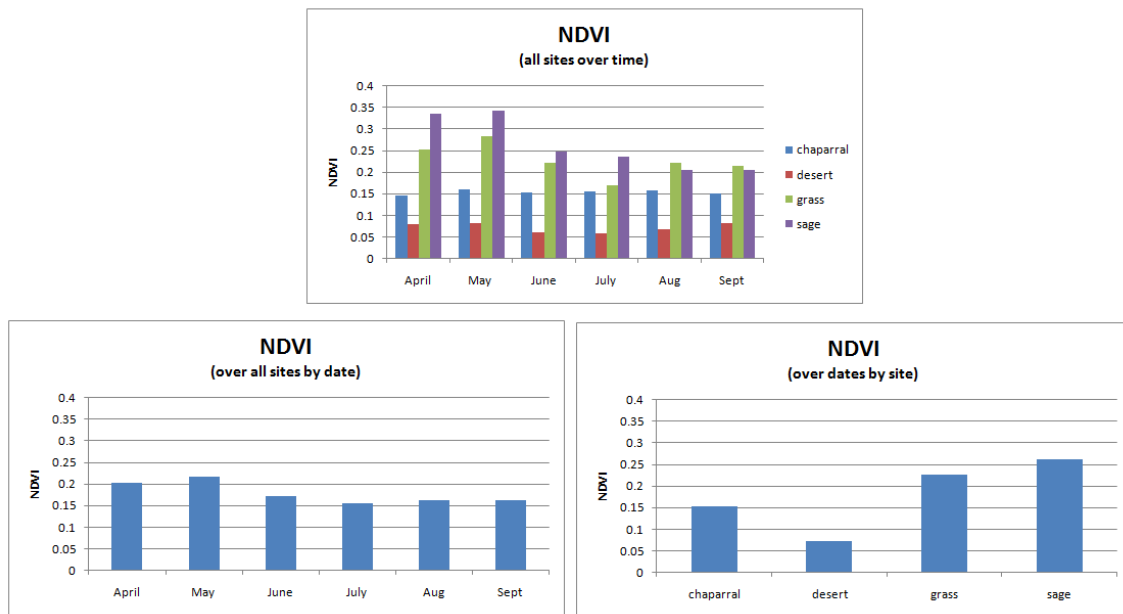


Figure 25: NDVI for all sites over time, averaged over all sites by date, and averaged over all dates by site. Note the substantial drop in NDVI over the summer for the Grass and Sage sites.

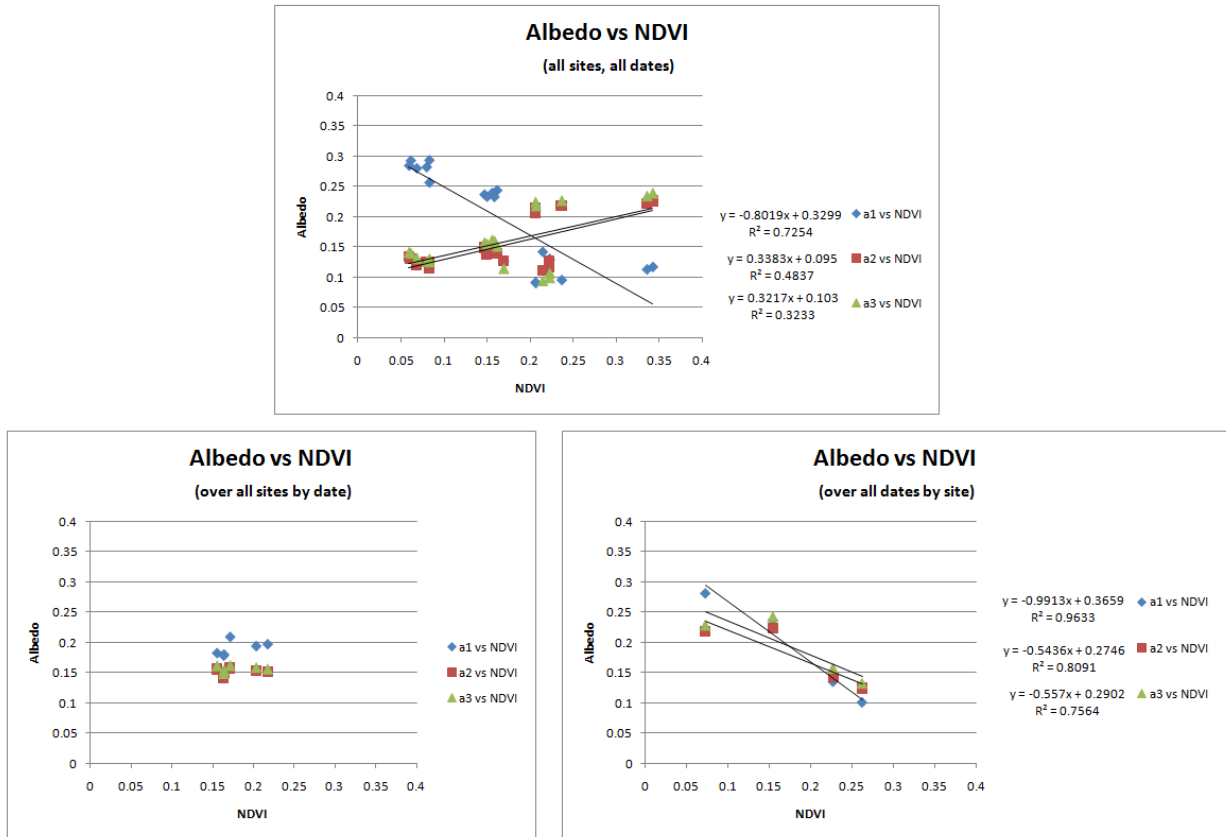


Figure 26: Albedo versus NDVI for all sites over time, averaged over all sites by date, and averaged over all dates by site. Note the lack of correlation between albedo and NDVI for over time.

5 Satellite Contributions to Surface Heat Budgets

Part of the original objectives of this work was to determine what satellites can contribute to budget studies. The flux tower footprint, which is a measure of the surface area that influences measured vertical turbulence in eddy covariance methods, is approximately 1 km² (Wang et al., 2006). The downward facing pyranometer measures reflected solar radiation over a much smaller surface area. The satellite measures of albedo, NDVI, and surface temperature are a better choice than the ground data estimates of these parameters because the satellite’s spatial resolution is a closer match to the towers’ turbulent flux footprint (Gash, 1986; Wang et al., 2006).

Another advantage of satellite is that they provide multispectral information about the surface. Most towers do not have spectrometers, which measure reflectivity across an extended portion of the electromagnetic spectrum. Such information is especially useful for monitoring vegetation and

moisture. Many of the towers in the Ameriflux network are equipped with sensors that measure the carbon flux and therefore, the state of the vegetation. However, if one is interested in monitoring the vegetation via radiative methods, one would require reflectivity information from the visible, near-, mid-, and thermal-infrared portions of the electromagnetic spectrum. From satellites, one could use the NDVI to monitor vegetation health and density, and the NDMI (Normalized Difference Moisture Index) to monitor the presence moisture across the scene of interest.

Finally, satellites also provide albedo, surface temperature, and multispectral indices such as NDVI or NDMI for a continuous region. This is especially useful in areas with very sparse or no available ground data. From ground data alone, one must extrapolate several point values to the larger, extended scene of interest. This extrapolation is not always accurate, especially in scenes with heterogeneous vegetation cover, moisture and terrain.

6 Conclusions

Both satellite and ground data were employed in examining several methods for calculating the terms of the surface heat budget in the semi-arid region of Southern California. The focus of the study was to investigate the seasonal impact and contribution of the landscape to the surface heat budget. This was accomplished by comparing variations in the surface heat budget terms and imbalances between and within six Landsat-5 TM 2007 images. The main objectives were to determine what satellites contribute to surface heat budget estimates, to determine whether surface heat budgets exhibit indications of an albedo or latent heat feedback, and to determine whether surface heat budgets vary significantly between areas of different vegetation cover. It was found that satellite measures of albedo, NDVI and surface temperature may be better than the ground estimates of these parameters because the satellite's spatial scale is closer to the towers' turbulent flux footprint (Gash, 1968, Wang et al., 2006). There is some variation between the various ground and satellite heat budget calculation methods. This discrepancy may be reduced in future studies with atmospheric corrections of the satellite images. However, there is very good agreement between the two satellite methods. Average values for the heat budget terms compare to those found in other studies (Tanaka et al., 2001). Though no evidence was found of an albedo or latent heat feedback, the heat budget does show a strong seasonal pattern in the sensible heat flux. Furthermore, the albedo, net radiation, ground storage flux and sensible heat flux are influenced significantly by vegetation cover density.

Possible extensions to this project could include efforts to incorporate additional satellite images from other years, and to apply the calculation of the heat budget terms to the entire image,

rather than at a few points with flux towers. Additional images of the same scene from other years would assist in investigating whether the results from this study are consistent with other summer seasons. Expanding the heat budget terms to cover the entire scene would require the creation of land cover classification maps. Care would have to be taken to ensure that ground measures such as air temperature, incoming solar radiation, reflected solar radiation, net radiation and the turbulent heat fluxes are assigned to the appropriate land cover classes.

An additional possibility would be to investigate other methods to calculate the sensible and latent heat fluxes. The sensible heat flux could be estimated from air temperature data from the flux towers, surface temperature from the satellite, and assuming a constant surface roughness according to land cover type. This estimate must take care to minimize errors due to differences between the radiative surface temperature and aerodynamic surface temperature as other studies have found that small errors in these variables quickly propagate to large errors in the sensible and latent heat flux (Chehbouni et al., 1997; Cleugh et al., 2007; Pielke and Avissar, 1990; Wang and Liang, 2008). The latent heat flux could be derived from the sensible heat flux and the Bowen ratio, which varies according to land cover and climate conditions. This would further test the various turbulent flux calculation methods.

Acknowledgements

The data from the Ameriflux tower network was used with permission by Mike Goulden, the primary investigator of the Southern California climate gradient sites.

References

“Ameriflux Network”, <http://public.ornl.gov/ameriflux/>

Bastiaanssen, W.G.M., Regionalization of surface flux densities and moisture indicators in composite terrain, *PhD thesis: Wageningen Agricultural University, Wageningen, the Netherlands, 143-161 (1995).*

Bates, B.C., Z.W. Kundzewicz, S.Wu and J.P. Palutikof, Eds., 2008: Climate Change and Water. Technical Paper of the Intergovernmental Panel on Climate Change, IPCC, Secretariat, Geneva, 210 pp.

Brivio, P.A., R. Colombo, and M. Meroni, The Use of Remotely-sensed Data for the Estimation of Energy Balance Components in a Mountainous Catchment Area, *Remote Sensing and Climate Modeling: Synergies and Limitations*, 307-327 (2001).

Brutsaert, W., On a Derivable Formula for Long-Wave Radiation From Clear Skies, *Water Resources Research*, **11**, 742-744, (1975).

Chander, G. and B. Markham, Revised Landsat-5 TM Radiometric Calibration Procedure and Postcalibration Dynamic Ranges, *IEEE Transactions on Geoscience and Remote Sensing*, **41**, 2674-2677 (2003).

Charney, J.G., Dynamics of deserts and drought in the Sahel, *Quarterly Journal of the Royal Meteorological Society*, **101**, 193-202, (1975).

Chehbouni, A., D. Lo Seen, E.G. Njoku, J.-P. Lhomme, B. Monteny, Y. H. Herr, Estimation of sensible heat flux over sparsely vegetated surfaces, *Journal of Hydrology*, 855-868 (1997).

Christensen, J.H., B. Hewitson, A. Busuioc, A. Chen, X. Gao, I. Held, R. Jones, R.K. Kolli, W. -T. Kwon, R. Laprise, V. Magaña Rueda, L. Mearns, C.G. Menéndez, J. Räisänen, A. Rinke, A. Sarr and P. Whetton, 2007: Regional Climate Projections. In: *Climate Change 2007: The Physical Science Basis. Contribution of Working Group I to the Fourth Assessment Report of the Intergovernmental Panel on Climate Change* [Solomon, S., D. Qin, M. Manning, Z. Chen, M. Marquis, K.B. Averyt, M. Tignor and H.L. Miller (eds.)]. Cambridge University Press, Cambridge, United Kingdom and New York, NY, USA.

Chodhury, B.J. and J.L. Monteith, A four-layer model for the heat budget of homogeneous land surfaces, *Quart. J. Roy. Meteor. Soc.*, **114**, 373-398 (1988).

Cleugh, H.A., R. Leuning, Q. Mu, S.W. Running, Regional evaporation estimates from flux tower and MODIS satellite data, *Remote Sensing of Environment*, **106**, 285-304 (2007).

COHA Causes of Haze Assessment, Joshua Tree Wilderness Area
http://www.coha.dri.edu/web/state_analysis/California/JoshuaTreeWA_metdsc.html, (November 13, 2004)

Dahm, C.N., J.R. Cleverly, J.E. Allred Coonrod, J.R. Thibault, D.E. McDonnell, D.J. Gilroy, Evapotranspiration at the land/water interface in a semi-arid drainage basin, *Freshwater Biology*, **47**, 831-843, (2002).

Daughtry, C.S.T., W.P. Kautas, M.S. Moran, P.J. Pinter, R.D. Jackson, P.W. Brown, W.D. Nichols and L.W. Gay, Spectral estimates of net radiation and soil heat flux, *Remote Sens. Environ.*, **32**, 111-124 (1990).

Dickinson, R.E. and A. Henderson-Sellers, Quart, Modelling tropical deforestation: A study of GCM land-surface parametrizations, *J. Roy. Meteor. Soc.*, **114**, 439-462, (1988).

Durre, I., J.M. Wallace, D.P. Lettenmair, Dependence of Extreme Daily Maximum Temperatures on Antecedent Soil Moisture in the Contiguous United States during Summer, *Journal of Climate*, **13**, 2641-2651, (2000).

Fu, P. and P.M. Rich. The Solar Analyst 1.0 Manual. Helios Environmental Modeling I, Institute (HEMI), USA, 2000.

Fu, P., and P.M. Rich, P.M., A geometric solar radiation model with applications in agriculture and forestry, *Computers and Electronics in Agriculture*, **37**, 25-35, (2002).

Gash, J.H.C., A Note on Estimating the Effect of a Limited Fetch on Micrometeorological Evaporation Measurements, *Boundary-Layer Meteorol.*, **35**, 409-413, (1986).

Lee, X., On micrometeorological observations of surface-air exchange over tall vegetation, *Agric. For. Meteorol.*, **91**, 39-49 (1998).

Lhomme, J.-P., A. Chehbouni, and B. Monteny, Effective parameters of surface energy balance in heterogeneous landscape, *Bound. Layer Meteorol.*, **71**, 297-310 (1994).

Liang, S., Narrowband to broadband conversions of land surface albedo I algorithms, *Remote Sensing of Environment*, **76**, 213-233, (2003).

Lillesand, T.M., R.W. Kiefer, J.W. Chipman. Remote Sensing and Image Interpretation, 5th Ed. John Wiley & Sons, Inc., 2004

Liou, K.N., An Introduction to Atmospheric Radiation, 2nd Edition. International Geophysics Series, Vol 84, Academic Press, 2002.

Lyons, T.J., P. Schwerdtfeger, J.M. Hacker, I.J. Foster, R.C.G. Smith, and H. Xinmei, Land-Atmosphere Interaction in a Semiarid Region: The Bunny Fence Experiment, *Bulletin of the American Meteorological Society*, **74**, 1327-1334, (1993).

Ma, Y., O. Tsukamoto, H. Isikawa, Z. Su, M. Menenti, J. Wang, and J. Wen., Determinations of Regional Land Surface Heat Flux Distributions over Heterogeneous Landscape of HEIFE Integrating Satellite Remote Sensing with Field Observations, *Journal of the Meteorological Society of Japan*, **80**, (2002).

Ma, Y., J. Wang, R. Huang, G. Wei, M. Menenti, Z. Su, Z. Hu, F. Gao, J. Wen, Remote Sensing Parameterization of Land Surface Heat Fluxes over Arid and Semi-arid Areas, *Advances in Atmospheric Sciences*, **20**, (2003).

Ma, Y., M. Menenti, O. Tsukamoto, H. Ishikawa, J. Wang, Q. Gao, Remote sensing parameterization of regional land surface heat fluxes over arid area in northwestern China, *Journal of Arid Environments*, **57**, 117-133 (2004).

Ma, Y., L. Zhong, Z. Su, H. Ishikawa, M. Menenti, and T. Koike, Determination of regional distributions and seasonal variations of land surface heat fluxes from Landsat-7 Enhanced Thematic Mapper data over the central Tibetan Plateau area, *Journal of Geophysical Research*, **111**, (2006)

Mahfouf, J.-F, Analysis of Soil Moisture from Near-Surface Parameters: A Feasibility Study, *Journal of Applied Meteorology*, **30**, 1534-1547, (1991).

Malek, E, Evaluation of effective atmospheric emissivity and parameterization of cloud at local scale, *Atmospheric Research*, **45**, 41-55, (1997).

Malek, E. and G.E. Bingham, Partitioning of radiation and energy balance components in an inhomogeneous desert valley, *Journal of Arid Environments*, **37**, 193-207 (1997).

Ocheltree, T.W. and H.W. Loescher, Design of the Ameriflux Portable Eddy Covariance System and Uncertainty Analysis of Carbon Measurements, *Journal of Atmospheric and Oceanic Technology*, **24**, 1389-1406, (2007).

Pielke, R.A. and R. Avissar, Influence of landscape structure on local and regional climate, *Landscape Ecology*, **4**, 33-155 (1990).

Tanaka, K., H. Ishikawa, T. Hayashi, I. Tamagawa, and Y. Ma, Surface Energy Budget at Amdo on the Tibetan Plateau using GAME/Tibet IOP98 Data, *Journal of the Meteorological Society of Japan*, **79**, 505-517 (2001).

Tasumi, M., R.G. Allen, R. Trezza, At-Surface Reflectance and Albedo from Satellite for Operational Calculation of Land Surface Energy Balance, *Journal of Hydrological Engineering*, **13**, 51-63, (2008).

Rabin, R.M., S. Stadler, P.J. Wetzel, D.J. Stensrud, M. Gregory, Observed Effects of Landscapes Variability on Convective Clouds, *American Meteorological Society*, **71**, 272-280, (1990).

Staley, D.O., and G. M. Jurica, Effective Atmospheric Emissivity under Clear Skies, *Journal of Applied Meteorology*, **11**, 349-356, (1972).

Valor, E. and V. Casselles, Mapping land surface emissivity from NDVI: application to European, African and South American Area, *Remote Sens. Environ.*, **57**, 167-184 (1996).

van den Hurk, B., Energy balanced based surface flux estimation from satellite stat, and its application for surface moisture assimilation

Verhoef, W., Theory of radiative transfer models applied to in optical remote sensing of vegetation canopies, *PhD thesis: Remote Sensing Department of National Aerospace Laboratory*, The Netherlands (1997).

Vermote, E.D., J.L. Tanré, M. Deuzé, J.J. Moncette, Second Simulation of the Satellite Signal in the Solar Spectrum (6S), User Guide, NASA GSFC, Greenbelt MD, USA.

Watson, R.T, M.C. Zinyowera, R.H. Moss, D.J. Dokken Eds., 1997: Summary for Policymakers, The Regional Impacts of Climate Change: An Assessment of Vulnerability, IPCC, Geneva, Switzerland, 16 pp.

Wang, J., K. Sahashi, E. Oktaki, T. Maitani, O. Tsukamoto, Y. Mistsuta, T. Kobayashi, H. Zhang, Q. Li, and A. Xie, Energy and mass transfer characteristics of soil-vegetation-atmosphere system in oasis area – Outline of the bio meteorological observation period (BOP), *Proceedings of International Symposium on HEIFE*, Nov. 8-11, Kyoto, 507-514 (1993).

Wang, W., K.J. Davis, D.M. Riccicuto, and M.P. Butler, An Approximate Footprint Model for Flux Measurements in the Convective Boundary Layer, *Journal of Atmospheric and Oceanic Technology*, **23**, 1384-1394, (2006).

Wang, K., and S. Liang, An Improved Method for Estimating Global Evapotranspiration Based on Satellite Determination of Surface Net Radiation, Vegetation Index, Temperature and Soil Moisture, *Journal of Hydrometeorology*, **9**, (2008).

Xu, Y., The Impact of Desertification in the Mongolian and the Inner Mongolian Grassland on the Regional Climate, *Journal of Climate*, **9**, 2173-2189 (1996).

Xu, J. and S. Haginoya, An Estimation of Heat and Water Balances in the Tibetan Plateau, *Journal of the Meteorological Society of Japan*, **79**, 485-504 (2001).

Zaitchik, B.F., A.L. Macalady, L.R. Bonneau, R.B. Smith, Europe's 2003 Heat Wave: A Satellite View of Impacts and Land-Atmosphere Feedbacks, *International Journal of Climatology*, **26**, 743-769, (2006).

Zhou, L., R.E. Dickinson, Y. Tian, M. Jin, K. Ogawa, H. Yu, and T. Schmugge, A sensitivity study of climate and energy balance with the use of satellite-derived emissivity data over Northern Africa and the Arabian Peninsula, *Journal of Geophysical Research*, **108**, (2003).

Appendix A: List of Acronyms, Variables and Symbols

Acronym	
DEM	Digital Elevation Model
DN	Digital Number
ET	Evapotranspiration
GCM	General Circulation Model
SRTM	Shuttle Radar Topography Mission
NDVI	Normalized Difference Vegetation Index
NDMI	Normalized Difference Moisture Index

Heat Budget Term Symbol	
S1	Incoming solar radiation from ground tower
S2	Incoming solar radiation estimated from solar zenith angle and atmospheric transmissivity
a1	Albedo calculated from tower measurements

a2	Albedo calculated from the weighted average of the satellite reflectance bands
a3	Albedo calculated from the average of the satellite reflectance bands
B1	Absorbed solar radiation calculated from s1 and a1
B2	Absorbed solar radiation calculated from s2 and a2
B3	Absorbed solar radiation calculated from s2 and a3
RS	Long-wave radiation emitted from the surface
RA	Long-wave radiation emitted by the atmosphere
RN1	Net radiation measured by the tower
RN2	Net radiation calculated from B2
RN3	Net radiation calculated from N3
H	Sensible heat flux
L	Latent heat flux
G1	Ground storage flux calculated from RN1
G2	Ground storage flux calculated from RN2
G3	Ground storage flux calculated from RN3

Additional Variables & Symbols	
S ₀	Solar constant (W/m ²)
s	Solar zenith angle (radian)
t ₀	Atmospheric transmissivity ~ 0.75 (Liou, 2002)
ρ	Planetary reflectance for the th band

	Stefan-Boltzmann constant ($5.67 \times 10^{-8} \text{ W/m}^2\text{K}^4$)
s	Surface emissivity ~ 0.95 (Lillisand, 2004; Malek and Bingham, 1997)
A	Atmospheric emissivity ~ 0.67 (Staley and Jurica, 1972; Brutsaert, 1975; Malek, 1997)
T_s	Surface temperature derived from satellite thermal band (K)
T_A	Temperature near the surface, measured by the flux tower (K)
ρ_a	Air density (kg/m^3)
C_p	Specific heat ($\text{J/kg}\cdot\text{K}$)
W	Vertical wind speed (m/s)
L	Latent heat of vaporization (J/kg)
Q	Specific humidity (kg/kg)

Appendix B: Landsat-5 TM Pre-processing (Chander and Markham, 2003)

Conversion of Digital Numbers (DN) to Radiance:

$$L_\lambda = \left(\frac{LMAX_\lambda - LMIN_\lambda}{Q_{cal\ max}} \right) Q_{cal} + LMIN_\lambda, \quad (A)$$

where L_λ is the spectral radiance ($\text{W/m}^2\cdot\text{sr}\cdot\mu\text{m}$), Q_{cal} is the pixel value (raw DN), $Q_{cal\ max}$ is the maximum DN value (255), $LMIN_\lambda$ is the spectral radiance ($\text{W/m}^2\cdot\text{sr}\cdot\mu\text{m}$) scaled to the minimum DN value (0) and $LMAX_\lambda$ is the spectral radiance ($\text{W/m}^2\cdot\text{sr}\cdot\mu\text{m}$) scaled to $Q_{cal\ max}$.

Landsat band number and wavelength range	$LMIN_\lambda$	$LMAX_\lambda$
Band 1 (0.45-0.52 μm)	-1.52	193.0
Band 2 (0.52-0.60 μm)	-2.84	365.0
Band 3 (0.63-0.69 μm)	-1.17	264.0

Band 4 (0.76-0.90μm)	-1.51	221.0
Band 5 (1.55-1.74μm)	-0.37	30.2
Band 6 (10.40-12.50μm)	1.2378	15.303
Band 7 (2.08-2.35μm)	-0.15	16.5

Table A: Landsat-5 TM Spectral Radiances for $L_{MIN\lambda}$ and $L_{MAX\lambda}$ in $W/m^2*sr*\mu m$

Radiance to Reflectance:

$$\rho_p = \frac{\pi * L_\lambda * d^2}{ESUN_\lambda * \cos(\theta_s)}, \quad (B)$$

where ρ_p is the planetary reflectance (unitless), L_λ is the spectral radiance, d is the earth-sun distance in astronomical units, $ESUN_\lambda$ is the mean solar exoatmospheric irradiance, and θ_s is the solar zenith angle (in degrees).

Landsat band number and wavelength range	ESUN
Band 1 (0.45-0.52μm)	1957
Band 2 (0.52-0.60μm)	1826
Band 3 (0.63-0.69μm)	1554
Band 4 (0.76-0.90μm)	1036
Band 5 (1.55-1.74μm)	215.0
Band 7 (2.08-2.35μm)	80.67

Table B: Landsat-5 TM Solar Exoatmospheric Spectral Irradiances (ESUN = $W/m^2*\mu m$)

Landsat-5 TM Band 6 Temperature:

$$T = \frac{K2}{\ln\left(\frac{K1}{L_\lambda} + 1\right)}, \quad (C)$$

where T is the surface brightness temperature (Kelvin), K2 is calibration constant 2 (Kelvin), K1 is calibration constant 1 ($W/m^2*sr*\mu m$), and L_λ is the spectral radiance.

K1 ($W/m^2*sr*\mu m$)	K2 (Kelvin)
607.76	1260.56

Table C: Landsat-5 TM thermal band calibration constants

Appendix C: Ameriflux Site Land-Cover Classifications and Vegetation Types

Site	International Geosphere-Biosphere Programme (IGBP) classification	Notes	Characteristic plant species
Chaparral	Open Shrublands	<ul style="list-style-type: none"> - Chaparral is considered to be a variety of woody shrubs ~1.3-3m in height adapted to drought and fire - This vegetation thrives in regions with mild temperature, limited winter rain, and hot dry summers - Chaparral vegetation cover ranges from San Benito County and Kern County to northern Ventura County and Santa Barbara county - Chaparral also typically ranges from ~32-60 deg N in the mountain regions 	<ul style="list-style-type: none"> - Juniperus californica - Erigonum fasciculatum
Desert	Barren or Sparsely Vegetated	<ul style="list-style-type: none"> - This site is located in the Mojave desert, which is surrounded by the San Bernardino Mountains to the north, the Santa Rosa Mountains to the south, the San Jacinto Mountains to the west and the Little San Bernardino Mountains to the east - The climate is generally very hot and dry year round 	<ul style="list-style-type: none"> - Salvia mohavensis - Yucca schidigera - Yucca brevifolia - Washintonia filifera
Grass	Grasslands	<ul style="list-style-type: none"> - The vegetation at this site may consist of a community of various grass species characteristic to the Pacific coast of 	<ul style="list-style-type: none"> - Dantonina - Festuca - Pteridium

		<p>California</p> <ul style="list-style-type: none"> - Many invasive species may also be present in this ecosystem 	<ul style="list-style-type: none"> - aquilinum - Iris douglasiana - Holcus lantatus (invasive)
Sage	Open Shrublands	<ul style="list-style-type: none"> - Sage is a low growing aromatic with drought-deciduous leaves, adapted to a semi-arid Mediterranean climate - The sage plants located along the coast of California are often described as a type of California chaparral - This type of chaparral is a collection of shrub plants which are native to coastal California and the northern region of Baja California 	<ul style="list-style-type: none"> - Artemisia californica - Salvia mellifera - Slavia aliana - Eriogonum fasciculatum - eriophyllum